EUROPEAN RESPIRATORY *journal*

FLAGSHIP SCIENTIFIC JOURNAL OF ERS

Early View

Original research article

Inspiratory hyperoxia suppresses lung cancer metastasis through a MYC/SLC1A5-dependent metabolic pathway

Xiucheng Liu, Hao Qin, Zheng Li, Yin Lv, Shoujie Feng, Wei Zhuang, Xiaoyu Quan, Chen Guo, Chang Chen, Hao Zhang

Please cite this article as: Liu X, Qin H, Li Z, *et al*. Inspiratory hyperoxia suppresses lung cancer metastasis through a MYC/SLC1A5-dependent metabolic pathway. *Eur Respir J* 2022; in press (https://doi.org/10.1183/13993003.00062-2022).

Inspiratory hyperoxia suppresses lung cancer metastasis through a MYC/SLC1A5-dependent metabolic pathway

Authors: Xiucheng Liu[1,2,3,4†], Hao Qin[2†], Zheng Li[5†], Yin Lv[2], Shoujie Feng[2], Wei Zhuang[6], Xiaoyu Quan[2], Chen Guo[2], Chang Chen[3,4*], Hao Zhang[1,2*]

Affiliations:

[1]Thoracic Surgery Laboratory, the First College of Clinical Medicine, Xuzhou Medical University, Xuzhou, Jiangsu 221006, China

[2]Department of Thoracic Surgery, Affiliated Hospital of Xuzhou Medical University, 99 West Huaihai Road, Xuzhou 221006, Jiangsu, China

[3]Shanghai Engineering Research Center of Lung Transplantation, Shanghai 200433, China

[4]Department of Thoracic Surgery, Shanghai Pulmonary Hospital, Tongji University School of Medicine, Shanghai, 200433, China

[5]Department of Thoracic Surgery, Huadong Hospital Affiliated to FuDan University, Shanghai, 200040, China

[6]Shanghai Key Laboratory of Signaling and Disease Research, School of Life Sciences and Technology, Tongji University, Shanghai 200092, China.

[†]These authors contributed equally to this work.

*Corresponding author:

Hao Zhang, PhD

Department of Thoracic Surgery, Affiliated Hospital of Xuzhou Medical University

Email: zhanghao@xzmu.edu.cn

Phone:+86-18798835177

& Chang Chen, PhD

Department of Thoracic Surgery, Shanghai Pulmonary Hospital, Tongji University School of Medicine, Shanghai 200433, China.

Email: chenthoracic@163.com

Abstract

The lack of knowledge about the effect of inspiratory hyperoxia (IH) on the lung-specific tumor microenvironment and progression of lung cancer has attracted considerable attention. This study proposes that IH has special significance for the malignant phenotype of lung cancer cells. The effects of different oxygenation parameters on the proliferation, apoptosis, invasion and migration of lung cancer cells were systematically evaluated *in vitro* and *in vivo*. Our results reveal that IH treatment (60% O_2, 6h/day) not only has no tumor progression-promoting effects, but also suppresses lung cancer metastasis and promotes long-term survival. We also combined transcriptome, proteome and metabolome analysis and found that hyperoxia treatment induced significant intracellular metabolic changes in lung cancer cells. Overall, we established that MYC/SLC1A5-induced metabolic reprogramming and glutamine addiction is a new mechanism that drives lung cancer metastasis, which can be significantly suppressed by IH treatment. These findings are relevant to the debate on the perils, promises and antitumor effect of IH, especially for patients with lung cancer.

Introduction

The tissue of tumor origin is a crucial factor determining the intrinsic malignant phenotype of a tumor and the characteristics of external tumor microenvironment (TME)[1-3]. Tumors originating in the same organ usually have similar gene expression signatures since they retain the transcriptional features of the parental tissue. The tissue of origin can also create an organ-specific TME for cancer cells, including epigenetically regulated gene expression,

cellular composition and tissue architecture[4, 5]. The TME with organ-specific characteristics will impose a variety of non-cell independent pressures on cancer cells and participate in the regulation of tumor initiation, progression, and metastasis. Notably, the TME of lung tumors is extremely unique due to distinct environment created by the gas exchange in which the oxygen concentration is constantly changing[6, 7]. However, although this must be an acute challenge to lung tumors, few studies have been conducted to explain the impact of this lung-specific TME on the progression of lung cancer.

The prognosis of patients with lung cancer remains dismal due to its aggressive malignancy and profound resistance to various forms of therapy. Thus, there is a strong impetus to identify new therapeutic targets for lung cancer. Inspiratory hyperoxia (IH) has been widely used as an adjuvant therapy in many clinical settings[8]. The effect of IH on cancer growth and metastasis remains controversial, especially in lung cancer. Existing studies have reported that, due to its ability to improve the oxygenation status of tumors, IH can be used in conjunction with radiotherapy or chemotherapy, but this application also raises concerns that an increased oxygen pressure may stimulate tumor growth via reoxygenation of hypoxic tumor cells and increased neovascularization[9-11]. Recently, Hatfield *et al*.[12] suggested that supplemental oxygenation (60%) can weaken the hypoxia-driven and adenosine A2A receptor or adenosine A2B receptor (A2AR/A2BR)-mediated (hypoxia-A2-adenosinergic) immunosuppression in the TME and serve as an immunological co-adjuvant in combination with current lung cancer immunotherapies. Notably, the effect of IH on the TME of lung tumors is comprehensive and subversive. Not only immune cells, but also mixed cells, including cancer cells, endothelial cells and

stromal cells, are under stress from lung-specific TME. Therefore, whether IH has anti- or pro-tumorigenic effect on lung tumors needs to be further studied.

In recent decades, the advanced metabolic analysis of cancer cells has expanded the understanding of the consequences and mechanisms of cancer metabolism in different stages of tumorigenesis[13, 14]. The classical oncogenic drivers, such as MYC, KRAS, *etc*., can induce metabolic reprogramming in cancer cells, which allows them to actively assist tumor growth and dissemination in nutrient- and oxygen-limited environments[15-17]. Glucose and glutamine are major anabolic carbon sources supporting cancer cell survival and biosynthesis in most tumors. In some malignant tumors, aberrantly activated oncogenes drive cancer cells into a state of nutritional addiction or to use unconventional nutritional catabolism pathways, such as the Warburg effect and glutamine addiction[18]. Recent studies have shown that the metabolic phenotype of tumors is also affected by the organ of origin and TME. An excellent example is that MYC activates glutamine catabolism in lung tumors, but in liver tumors it activates glutamine synthesis [19].

Here, we hypothesized that the change in oxygen concentration is of unique significance to the TME and the malignant phenotype of lung tumor cells. To confirm this hypothesis, in this study the effects of different oxygenation parameters on the proliferation, apoptosis, invasion and migration of lung cancer cells were systematically evaluated *in vitro* and *in vivo*. Transcriptome, proteome, and metabolome analysis were combined to determine the effect of supplemental oxygen on the malignant phenotype of lung cancer and the detailed undelying mechanism. The findings of this study will provide an adequate theoretical basis to clarify the safety of oxygenation therapy for lung cancer patients and ascertain whether

it has the potential to be used as an adjuvant in combination with current lung cancer treatment methods.

Results

1. Inspiratory hyperoxia suppresses lung cancer metastasis.

To determine the effects of long-term IH on lung cancer cell, we established a lung cancer model in immunodeficient mice. Using a gas control delivery system, mice were exposed to various concentrations of oxygen (21, 30, 60, 90 and 98% oxygen) to mimic protocols of supplemental oxygen delivery to humans (Fig. 1A). Tumor-free mice exposed to 98% oxygen (6h/day) had a mortality rate higher than 50% within 30 days. Such mortality rate may be the result of oxygen toxicity, nonspecific inflammatory responses and extensive alveolar hemorrhage (Fig. S1A, 1C). The survival of tumor-free mice exposed to 60% oxygen for less than 6 h was not affected. Histological examination revealed that about 14% of the mice exposed to 60% oxygen had non-fatal emphysema or pulmonary bulla (Fig. S1B, 1D). In addition, mice exposed to 60% oxygen showed no significant difference in general physical signs (heart rate, body temperature, and respiration rate) except for weight loss (Fig. S1E). In general, the exposure to 60% oxygen (＜6 h/day) proved to be safe in long-term treatment.

Tumor-bearing mice exposed to 60% oxygen (6h/day) showed significantly improved survival and suppressed lung tumor progression (Fig. 1B, 1C). The incidence of lymph node metastasis and distant metastasis in the control group was 2.5-fold and 4-fold higher than that in the IH exposed mice, respectively (Fig. 1D). Immunohistochemical (IHC)

staining showed that exposure to IH downregulated the expression of high mobility group AT-hook 2 (HMGA2) protein, which has been reported to be a marker of tumor metastasis (Fig. S1F)[20].

In Balb/c nude mice, IH also prevented LLC cells and H1299 cells from metastasizing to the lung and reduced the primary tumor burden and improved survival after intravenous (*i.v.*) injection (Fig. 1E-H). The results of a luciferase reporter assay using H1299 cells stably expressing firefly luciferase implanted into Balb/c nude mice by *i.v*. injection further confirmed that IH has antimetastatic effect (Fig. 1I).

2. Effects of Inspiratory hyperoxia on the proliferation, invasiveness and apoptosis of lung cancer cells.

To further evaluate the effects of IH on lung tissues and tumors, BEAS-2b, H1299, A549, H226 and LLC cells were cultured under high oxygen concentration (60% O_2, 5% CO_2, 35% N_2) to simulate IH *in vitro*. The measurement of the proliferation rate using the cell counting kit-8 (CCK-8) assay and 5-ethynyl-2'-deoxyuridine (EdU) incorporation showed that exposure to 60% oxygen for 24 h significantly reduced the proliferation rate of human normal lung epithelial cells (BEAS-2b cell line), human lung cancer cells (H1299, A549 and H226 cell lines) and LLC cells (Fig. S2A-F). However, it did not alter the growth of primary tumors when H1299 cells were injected subcutaneously into the mice (Fig. S2G, 2H). Experiments using hypoxia reagent to label hypoxia area in primary tumors revealed that IH did not effectively reduce or reverse the hypoxic area in tumor xenografts (Fig. S2I). These data suggest that the inhibition of lung tumor growth by IH may be closely related to lung specific TME.

In addition, exposure to hyperoxia for less than 24 h had no effect on apoptosis and necrosis in BEAS-2b and lung cancer cell lines, but in BEAS-2b, LLC, H1299, H226 and A549 cells exposed to 60% oxygen for more than 48 h induced significant apoptosis and necrosis (Fig. S3). Cell migration, invasion and scratch assays showed that lung cancer cells exposed to 60% oxygen had lower invasive and migratory abilities (Fig. S4).

3. Transcriptomic and proteomic profiling of hyperoxia exposed H1299 cells.

RNA sequencing (RNA-seq, GEO: GSE192839) and tandem mass tag (TMT)-based quantitative proteomics analyses (iProX data licence: IPX0003908000) on controls and 60% oxygen (24 h) exposed H1299 cells were performed, and 59, 577 RNAs and 5, 970 proteins were identified, respectively (Fig. 2A, 2B). The expression levels of 5, 460 identified proteins and their corresponding mRNAs showed a poor correlation (R^2= 0.0312, Fig. 2C, 2D). For mRNA and protein differential expression analyses, a false discovery rate (FDR) cut off of 5% and a 2-fold change threshold were used. When integrating these datasets, we identified 43 overlapping differentially expressed genes and proteins (Fig. 2E).

Gene ontology enrichment analysis revealed that these significantly differentially expressed genes and proteins were enriched in “carbohydrate metabolic process”, “trans-epithelial transport”, “ADP metabolic process” and cell motility and migration regulation process (Fig. 2F). Kyoto Encyclopedia of Genes and Genomes (KEGG) enrichment analysis revealed a marked enrichment in cell metabolism as well as pathways associated with cancer development (Fig. 2G). To identify cellular pathways involved in lung cancer metastasis and metabolism, Gene Set Enrichment Analysis (GSEA) performed on the RNA-seq data determined that, compared with control cells, cells exposed to hyperoxia

showed reduced enrichment of metastasis-related genes reported in the Human Cancer Metastasis Database (Fig. 2H)[21]. Furthermore, GSEA also revealed a significant decrease in metabolic pathways, including mitochondrial inner membrane, oxidative phosphorylation, glucose metabolism and glutamine metabolism genes, upon hyperoxia exposure (Fig. 2I, 2J, S5). In general, the multi-omics data suggested that exposure to 60% oxygen (24 h) may lead to significant metabolic reprogramming of lung cancer cells, which may explain its antitumor metastasis activity.

4. Metabolomic changes following hyperoxia treatment.

Our analysis of the cellular metabolome of normoxia and hyperoxia-exposed H1299 cells using untargeted metabolomics to establish a holistic overview of cancer metabolism mechanisms underlying hyperoxia treatment identified a total of 319 structurally named metabolite across both treatment groups. Compared with the normoxia group, in hyperoxia treated H1299 cells 13 metabolites, including 6-methylquinoline, hippuric acid and pyridoxal, were significantly increased, and 15 metabolites, including 4-hydroxybenzaldehyde, L-glutamine, asparagine and pyruvic acid, were significantly decreased (Fig. 3A-3G). Additionally, analysis of the KEGG metabolic library using the Metaboanalyst (3.0) software revealed that altered metabolites were enriched in “alanine, aspartate and glutamate metabolism”, “arginine biosynthesis”, “glyoxylate and dicarboxylate metabolism”, “TCA cycle” and “D-glutamine and D-glutamate metabolism” processes (Fig. 3H). It is known that glucose and glutamine are the main anabolic carbon sources that support tumor cell proliferation and invasion. Therefore, we hypothesize that hyperoxia exposure may cause changes in the metabolism of glutamine and glucose,

thereby regulating the metastasis of lung cancer.

5. Inspiratory hyperoxia decreases the glutamine uptake of lung tumor.

The assessment of the effect of hyperoxia on glutamine metabolism in lung cancer cells through measuring the level of intracellular glutamine by enzyme-linked immunosorbent assay (ELISA) revealed that hyperoxia exposure caused a continuous decrease in glutamine in H1299 and A549 cells (Fig. 4A-4C). Heat map and gene enrichment analysis indicated that the metabolic pathway of glutamine was inhibited in H1299 cells exposed to hyperoxia (Fig. 4D-4F). Quantitative real-time polymerase chain reaction (qRT-PCR) and immunoblotting analyses were used to confirm the regulatory effects of hyperoxia on the expression of genes largely involved in the transport, synthesis and catabolism of glutamine. The results indicated that solute carrier family 1 member 5 (SLC1A5), also known as ASCT2, a major glutamine transporter, which was highly expressed in normoxia H1299, A549, H226 and H520 cells was downregulated by 60% oxygen treatment (Fig. 4G-4J, S6).

In an *in vivo* lung metastasis mouse model, we found that SLC1A5 expression was significantly reduced in IH exposed lung tumors compared with that in the control group (Fig. 4K). However, 60% oxygen treatment had no effect on the expression of SLC1A5 in subcutaneously transplanted tumors in mice (Fig. 4L). We inferred that the IH-induced decrease in SLC1A5 expression in lung tumor led to reduced glutamine uptake and metabolic demands to regulate tumor metastasis. The measurement of glutamine uptake further confirmed that hyperoxia significantly decreased the intracellular transport of glutamine in lung cancer cells (Fig. 4M, 4N).

Furthermore, the level of glutathione was significantly increased in BEAS-2b cells treated with 60% oxygen, suggesting that hyperoxia may play a role in the maintenance of cellular redox homeostasis. However, the opposite effect on intracellular glutathione was observed in H1299 and A549 cells (Fig. S7A-7C). We speculate that the hyperoxia induced decrease of the glutamine level may lead to the obstruction of glutathione synthesis in lung cancer cells. Hyperoxia caused a more significant increase in reactive energy species (ROS) levels in lung cancer cells compared with BEAS-2b cells (Fig. S7D-7F). Remarkably, the treatment with the antioxidant N-acetylcysteine (NAC) could prevent the apoptosis caused by exposure to hyperoxia for more than 48 h, but promoted cancer progression (Fig. S7G-7I).

6. The progression of lung cancer depends on glucose and glutamine catabolism.

Non-small cell lung cancer (NSCLC) cells have been reported to use glycolysis as the main pathway of glucose catabolism, even in an oxygen enriched environment, that is, the Warburg effect[22]. Our metabolomic and transcriptomics data showed that exposure to hyperoxia leads to an increase in the heterogeneity of carbohydrate small molecule compounds and gene expression levels involved in glucose metabolism in lung cancer cells (Fig. S8A, 8B). We analyzed the protein expression levels of glycolysis related enzymes and found lower levels of HK2, PFK2 and MCT1 in H1299 and A549 cells exposed to 60% oxygen (24 h) compared to controls (Fig. S8C). The measurement of the oxygen consumption rate (OCR) and extracellular acidification rate (ECAR) in BEAS-2b, H1299 and A549 cells revealed that H1299 and A549 cells exposed to hyperoxia showed decreased basal and maximum ECAR and OCR compared to the control group (Fig. S8D-

8I). The glycolytic capacity of lung cancer cells exposed to 60% oxygen for 12 h was 40-50% lower than that in controls. However, hyperoxia did not significantly affect the glycolytic capacity and mitochondrial respiratory capacity of BEAS-2b cells (Fig. S8J-8O).

In addition, we also found that the proliferation and survival of both lung cancer cells and BEAS-2b cells are heavily dependent on glucose. Compared with glucose deprivation, glutamine deprivation is more associated with reducing the aggressiveness of tumor cells, but less with inducing proliferation arrest and apoptosis of BEAS-2b, H1299 and A549 cells (Fig. S9). These results suggest that antitumor strategies that target glutamine catabolism have greater safety and feasibility.

7. SLC1A5 mediates the hyperoxia-induced inhibition of glutamine catabolism.

Functional analysis of SLC1A5 showed that short hairpin RNA (shRNA)-mediated knockdown of SLC1A5 expression significantly decreased the proliferation of H1299, A549 and H226 cells (Fig. 5A-5C, S10) and reduced the migration and invasion abilities in H1299 cells (Fig. 5D, 5E). In *in vivo* metastasis assays, SLC1A5 knockdown significantly inhibited metastasis of H1299 cells to the lung and reduced the primary tumor burden (Fig. 5F-5H). Further investigation of the role of SLC1A5 in the growth of lung tumor in a mouse xenograft model indicated that a low expression level of SLC1A5 could reduce tumor weight and volume (Fig. 5I-5L). Moreover, SLC1A5 overexpression increased the level of intracellular glutamine in lung cancer cells and partially reverse the hyperoxia-induced inhibition of invasion (Fig. S11).

8. MYC directly activates SLC1A5 transcription.

The possible mechanism of the down-regulation of SLC1A5 was further investigated by

determining the expression of RNA-seq identified differentially expressed transcription factors by qRT-PCR and Western blotting analyses. The results showed that 60% oxygen exposure significantly reduced the level of MYC in H1299 and H226 cells (Fig. 6A-6C, S6). We proposed that the SLC1A5 gene may be a target of oncogenic MYC. The inactivation of C-MYC by JQ1 consistently reduced expression of SLC1A5 in H1299 and A549 cells. Similarly, MYC depletion led to the decrease of SLC1A5 expression in H1299 cells (Fig. 6D-6G). Among the 441 hyperoxia-induced differentially expressed genes, we identified a MYC-binding motif in the proximal promoters of 82 genes, including SLC1A5 (Fig. 6H, 6I). Analysis of a publicly available ChIP sequencing dataset (GSE80151) further suggested that SLC1A5 may be a MYC target gene. To determine whether the MYC-binding sequence participates in SLC1A5 transcriptional activation, we cloned the 400- to 500-bp promoter region containing the putative (wt) MYC binding sequence and a mutated (mut) version into the luciferase reporter vector (Fig. 6J). As expected, the luciferase activity from the SLC1A5 promoter was 2.5- fold higher in MYC-REwt than in RE-mut in 293T cells (Fig. 6K). The results of the ChIP-qPCR assay further confirmed the decreased MYC occupancy on the SLC1A5 promoter in H1299 and A549 cells treated with JQ1 or MYC knockdown (Fig. 6L-6O). Thus, the oncogene MYC activates transcription of SLC1A5, which raises the possibility that MYC regulates glutamine uptake.

9. SLC1A5 expression level is associated with tumor stage, lymph node metastases and poor survival in human NSCLC.

We performed microarray analysis using the Gene Expression Profiling Interactive Analysis (GEPIA) online platform and database to identify the expressions of SLC1A5 and

MYC in NSCLC. The results indicated that the SLC1A5 level was higher in NSCLC than in the adjacent tissues. Notably, MYC was only significantly expressed in lung squamous cell carcinoma (LUSC), and did not appear to play a significant role in lung adenocarcinoma (LUAD) (Fig. 7A-7D). Similar findings were also observed in cervical squamous cell carcinoma, cholangiocarcinoma, pancreatic cancer and other malignant tumors (Fig. S12A, 12B). In addition, there was a significant positive correlation between MYC and SLC1A5 mRNA levels in NSCLC (Fig. 7E, S12C, 12D). Analysis of The Cancer Genome Atlas (TCGA) datasets also showed that the levels of SLC1A5 and MYC were upregulated in LUAD with lymph node or distant metastasis (Fig. 7F-7I, S12E-12L).

We also constructed a tissue microarray (TMA) of 219 human NSCLC specimens, and used it for immunohistochemical (IHC) analysis (Fig. 7J). We found that the level of SLC1A5 was significantly associated with clinical tumor stage and lymph node metastasis in both LUAD and LUSC (Fig. 7K-7N, Supplementary Table 2, 3). Additionally, Kaplan–Meier analysis indicated that NSCLC patients with high levels of SLC1A5 have poor survival prognosis (Fig. 7O).

Discussion

In this study, we hypothesized that the change in oxygen concentration has a unique significance for the lung-specific TME and the malignant phenotype of lung tumor cells. To confirm such hypothesis, the effects of different oxygenation parameters on the proliferation, apoptosis, and invasion of lung cancer cells were systematically evaluated *in vitro* and *in vivo*. In addition, transcriptome, proteome, and metabolome analysis were

combined to determine the effect of supplemental oxygen on the malignant phenotype of lung cancer and the detailed mechanism mediating this effect. The findings of this study will provide a satisfactory theoretical basis to clarify the safety of oxygenation therapy for lung cancer patients and ascertain whether it has the potential to be used as an adjuvant in combination with current lung cancer treatment methods.

Effectively reducing tumor burden and metastasis risk is the main challenge in the clinical response and management of advanced lung cancer[23, 24].This study demonstrated that MYC/SLC1A5-induced metabolic reprogramming and glutamine addiction serves as a new mechanism that drives lung cancer metastasis, which can be significantly suppressed by IH (60% oxygen). These findings are relevant to the debate on the perils, promises and antitumor effect of IH, especially for patients with lung cancer. The clinical protocol of respiratory hyperoxia is widely used in patients with oxygenation deficiency caused by various diseases, including lung cancer. Previous studies have shown that respiratory hyperoxia has a confirmed stimulatory effect on the proliferation of endothelial and epithelial cells in wound healing[25-28]. However, the unknown impact of IH on local lung cancer progression has raised some concerns. Over the last decade, studies have strongly suggested that respiratory hyperoxia did not have a stimulatory effect on tumor growth, recurrence, and metastasis in most cancers[29]. Evidence from clinical and animal studies has shown that hyperbaric oxygen (HBO) can enhance the effects of chemotherapy and radiotherapy in cervical and breast cancer[30, 31]. A possible explanation is that HBO overcomes the hypoxia and insufficient vascular development inside the tumor, thereby increasing the transport of drug molecules and therapeutic sensitivity[32]. Recently, Kim *et*

al.[9] intravenously injected mice with LLC cells and exposed them to a 24 h-normobaric (95% oxygen)/normoxia cycle for two weeks, and found that respiratory hyperoxia inhibited the progression of lung cancer by inducing apoptosis. Additionally, studies by Hatfield *et al*. also revealed the antitumor effects of respiratory hyperoxia by reversing the hypoxia-adenosinergic immunosuppression in the TME[12, 33, 34]. In this study, our data indicated that exposure to 60% oxygen (6h/day) inhibited lung cancer metastasis and increased the survival time of tumor-bearing mice. We emphasize that it is very important to take the proper time of application, duration, pressure and dose to achieve the overall benefit for mice with lung tumors. It is not recommended to use more than 60% oxygen and a duration of more than 12 h, to avoid serious complications, including pulmonary bullae, alveolar hemorrhage, oxygen toxicity, and even death.

Glutamine is an essential amino acid for NSCLC growth *in vitro* and *in vivo*. Recent studies have proposed that glutamine supports lung cancer growth through a KRAS-regulated metabolic pathway under hypoxia[35, 36]. Momcilovic *et al*.[37] also showed that LUSC could circumvent inhibition of mTOR and glycolysis by upregulation of glutamine metabolism. Another major finding of our untargeted metabolomics study is that IH had a profound effect on intracellular metabolism of lung cancer cells. We found that hyperoxia exposure significantly decreased the expression of SLC1A5 and the level of intracellular glutamine in lung cancer cells. Additional data confirmed that hyperoxia-induced suppression of the aggressiveness of lung cancer is mediated by inhibition of glutamine uptake, in a manner similar to glutamine deprivation. *In vitro* study, hyperoxia-induced suppression of glycolysis may be the main contributor to its inhibition of the proliferation of

lung cancer cells and BEAS-2b cells. However, hyperoxia did not significantly affect the growth of tumor xenografts *in vivo*. We believe that there may be two reasons for this inconsistency. First, oxygen supplementation is not enough to counteract the limitations of tumor volume increase and vascular development defects. Second, the inhibitory effect of IH on lung tumor growth may depend on lung-specific TME. In fact, tumor cells cultured *in vitro* and early primary lung tumors do not experience significant hypoxia, which suggests that reversing hypoxia is not the main mechanism of hyperoxia-induced inhibition of the proliferation of lung cancer cells and reduction of the lung tumor burden.

The transcription factor MYC is one of the most common somatically mutated oncogenes in human cancer. High level of MYC is found in both high-grade premalignancy and invasive tumors and is associated with poor outcome in different human tumor types[38, 39]. Recent studies suggest that MYC is specifically necessary for the metastasis of tumor cells independent of its effects on proliferation and survival[40]. Our data indicated that exposure to 60% oxygen for 12 h significantly downregulated MYC expression at both mRNA and protein levels. Additionally, we found that MYC directly activates SLC1A5 transcription, leading to the reprogramming of glutamine metabolism. In summary, we discovered a MYC/SLC1A5 signaling pathway regulated by hyperoxia, which is the basis for glutamine uptake and lung cancer metastasis (Fig. 8).

Moreover, our preliminarily investigation of the role of IH-induced oxidative stress in the progression of lung cancer revealed that hyperoxia exposure caused a decrease in the glutathione level and a significant increase in intracellular ROS in BEAS-2b, H1299 and A549 cells. Recent studies provide compelling evidence that ROS have anti-tumorigenic

roles with the potential to become a novel anticancer target[41-44]. Our study also confirmed that exogenous antioxidants promote the metastasis of lung cancer under IH, which is consistent with previous reports[16]. However, exposure to hyperoxia for more than 48 h could significantly increase intracellular ROS to toxic levels and induced severe apoptosis and necrosis in both lung cancer cells and BEAS-2b cells. This reminds us that balancing the antitumor activity and toxic effect of ROS needs to be cautiously considered when using IH.

In conclusion, our study reveals that IH exposure not only has no tumor progression-inducing effects, but also suppresses lung cancer metastasis. We also propose that intracellular metabolic reprogramming driven by the oncogene MYC/SLC1A5 axis is the main mechanism by which IH inhibits cancer metastasis. These findings will have implications for future therapeutic approaches as IH can potentially synergize with therapies that target glutamine metabolism, glycolysis or ROS, such as chemotherapy, radiation and novel targeted drug.

Author contributions

H.Z and C.C conceived the project. X.C.L, H.Q, Z.L and X.C.Q performed all experiments on cell lines and mice. W.Z, S.J.F, C.G and Y.L helped establish lung cancer models. X.C.L, X.Y.Q, C.L.J and Z.X.C wrote the manuscript. All authors contributed to experimental design and data analysis. XCL composed the manuscript. All authors reviewed the manuscript and discussed the work.

Declaration of competing interests

The authors declare that they have no competing interests.

Acknowledgments

We thank Shanghai Aksomics Biotech Co. Ltd. (Shanghai, China) for assistance with the analysis of multiomics data. This work was supported by funds from the National Natural Science Foundation of China (81400227 to H.Z.), from the Social Development Projects of Key R&D Programs in Jiangsu Province (BE2019643 to H.Z.), from the National Natural Science Foundation of Jiangsu Province (BK20171178 to H.Z.), from General Program of Jiangsu Commission of Health (H2017083 to H.Z.), from the Project of Invigorating Health Care through Science, Technology and Education, Jiangsu Provincial Medical Youth Talent (QNRC2016778 to H.Z).

MATERIALS AND METHODS

Cell Lines

The immortalized human lung epithelial cell line BEAS-2b, Lewis lung carcinoma (LLC) cells and the human lung cancer cell lines H1299 and A549 were obtained from FuHeng Biology (Shanghai, China). Cells were cultured in Dulbecco's modified Eagle's medium (DMEM) or RPMI 1640 medium (Gibco/Thermo Fisher Scientific Inc., Waltham, MA, USA) supplemented with 10% fetal bovine serum, and 1% penicillin/streptomycin solution, in an incubator at 37 °C, with a humidified atmosphere containing 5% CO_2.

Mice

Balb/c nude mice (4-6 weeks old) were purchased from Beijing Weitong Lihua Laboratory Animal Technology Co., Ltd. (Beijing, China). All animal experiments were approved by the

Animal Protection and Utilization Committee of Xuzhou Medical University (Xuzhou, China). No preference in mouse sex was given for any of the studies.

Clinical samples

A series of tissue samples from patients with non-small cell lung cancer (NSCLC) who did not receive radiotherapy or chemotherapy were obtained from the Department of Pathology of Shanghai Pulmonary Hospital. All specimens were obtained under the guidance of the U.S. Health Insurance Portability and Accountability Act (HIPAA) protocol and supervised by the ethics committee of the hospital, and were pathologically confirmed as NSCLC.

Establishment of lung cancer model

An orthotopic lung tumor model was established as previously reported[45]. Briefly, Balb/c nude mice were anaesthetized with an intraperitoneal injection of sodium pentobarbital (60 mg/kg). After confirming that mice have been adequately anesthetized, LLC cells (1.0×10^6) with 50% Matrigel matrix (Corning Inc., Corning, NY, USA) were injected orthotopically into the left lung. Mice were examined daily for infection, bleeding, weight loss, lethargy, and changes in food and / or water consumption.

For the lung metastasis model, luciferase-labelled LLC and H1299 cells（$4x10^6$）were injected into mice through the tail vein. The fluorescence expression was detected after 1 months, and then the lungs were harvested.

Hyperoxic exposure

Mice were placed in an ATTENDOR animal gas control system (China Innovation Instrument Co., Ltd., Ningbo, China), and exposed to a well-controlled gas composition to

mimic protocols of supplemental oxygen delivery to humans. This system provides an independent environment with a controllable oxygen concentration for animals. The gas monitoring module can effectively control carbon dioxide emissions and supply gas of excellent quality for the breathing of mice. The oxygen concentrations of 21, 30, 60, 90 and 98% were selected and supplied to mice for 3, 6 and 12 h per day for 30 days.

A Smartor-118-three gas incubator (China Innovation Instrument Co., Ltd.) was used to mimic protocols of supplemental oxygen delivery *in vitro*. BEAS-2b, LLC, H1299, A549 and H226 cells were exposed to hyperoxia (60% O_2 / 5%CO_2 / 35%N_2) for 4, 8, 12, 24, 48 and 72 h.

Tumor xenograft study

H1299 cells (5×10^6) were injected subcutaneously into the flanks of mice. Then, mice in the hyperoxia group were treated with IH (60% oxygen) for 21 days, and the mice in the control group were routinely fed. Tumor volume (V) was monitored every 4 days by measuring the long axis (L) and the short axis (W) of xenograft tumors and calculated using the following formula: $V = (L \times W^2)/2$.

RNA sequencing analysis

Total RNA was isolated from the H1299 cells exposed to hyperoxia (60% O_2, 24 h) and control cells, quantified and its integrity checked. The high-throughput RNA sequencing analysis was performed by Shanghai Aksomics Biotech Co. Ltd. (Shanghai, China). Briefly, the ribosomal RNA (rRNA) was removed from the total RNA using the NEBNext® rRNA Depletion Kit (New England Biolabs, Inc., Ipswich, MA, USA) following the manufacturer's instructions. RNA libraries were constructed using the NEBNext® Ultra™ II Directional

RNA Library Prep Kit (New England Biolabs, Inc.) according to the manufacturer's instructions. Then, the HTSeq software (v0.9.1) was used to obtain the transcript level raw count as the expression profiling, and the edgeR software (v3.16.5) was used to perform normalization, and differentially expressed genes were identified by their p-value and expression fold change.

Liquid chromatography tandem Mass spectrometry (LC-MS/MS) for proteome analysis

H1299 cells (1.0×10^7) were lysed in 1,000 μL RIPA buffer at 4 °C. The total protein content of each sample was then determined using a bicinchoninic acid (BCA) protein assay. Then, after performing acetone precipitation and trypsin digestion, the samples were labeled with tandem mass tag (TMT). Subsequently, after removing the sodium deoxycholate (SDC) from the samples, the peptides were desalinated. After reverse-phase high-performance liquid chromatography (RP-HPLC), peptides were fractionated into 120 fractions using high pH RPRP-HPLC, and then combined into 8 fractions. For each fraction, ~2 μg peptide were separated and analyzed using a nano-UPLC (Easy-nLC 1200) coupled to Q-Exactive mass spectrometry (Thermo Fisher Scientific Inc.).

The original data obtained by liquid chromatography-tandem mass spectrometry (LC-MS/MS) were searched and quantified using the Max Quant software (version 1.5.6.0; Max-Planck-Institute of Biochemistry, Martinsried, Germany). The protein sequence database (Uniprot_organism_2016_09) was downloaded from UNIPROT. This database and its reverse decoy were then searched using the Max Quant software. Both peptide and protein FDR should be less than 0.01. Only unmodified unique peptides were used for

quantification. All the other parameters were kept as default.

Metabolomics

The 1260 infinity high-performance liquid chromatography (HPLC) system (Agilent Technologies Inc., Santa Clara, CA, USA) coupled with Q-Exactive MS/MS (Thermo Fisher Scientific Inc.) was used for metabolomics analysis in this study. Cells were washed twice with ammonium carbonate (75 mM) at pH 7.4 and snap frozen in liquid nitrogen. Metabolites were extracted with MeOH: acetonitrile (ACN) (1:1, v/v). The samples were incubated for 1 h at -20 °C, followed by 15 min centrifugation at 20,000 g and 4 °C to precipitate proteins. After drying and reconstituting with ACN: H_2O (1:1, v/v), the extracts were centrifuged for 15 min at 20,000 rpm to remove insoluble debris. Samples were stored at −80°C until LC/MS analysis.

For LC/MS analysis, samples were separated on an amide column with a mobile phase A consisting of water mixed with ammonium acetate (25 mM) and ammonium hydroxide (25 mM) and a mobile phase B consisting of ACN. The MS/MS analysis coupled with HPLC was performed on a Q-Exactive MS/MS system (Thermo Fisher Scientific Inc.). The different data-dependent analysis (DDA) methods were performed as follows: full scan range: 60 to 900 (m/z); resolution for MS1 and ddMS2: 70,000 and 17,500, respectively; maximum injection time for MS1 and ddMS2: 100 and 45 ms, respectively; automatic gain control (AGC) for MS1 and ddMS2: $3e^6$ and $2e^5$, respectively; isolation window: 1.6 m/z; normalized collision energies (NCE): 10, 17, 25 or 30, 40, 50. The full scan method was performed as follows: the full scan range was 60–900 (m/z); the AGC was $3e^6$ ions; resolution was 140,000; and the maximum injection time was 100 ms. Univariate analysis

was used to analysis the metabolomics dataset. The relative difference coefficient (*d* value) between groups was first calculated.

$$\mathrm{d} = \frac{\overline{X1} - \overline{X2}}{S - S0}.$$

(*X*1, the average content of a metabolite in H1299 cells cultured in normoxia; *X*2, the average content of a metabolite in H1299 cells with 60% oxygen treatment for 24 h; S, the sum of intra class variance; *S*0, correction value of *S*). Subsequently, significance analysis of microarrays (SAM) was used to identify deferentially expressed metabolites and to estimate the FDR.

Preparation of plasmids, lentivirus, and stable cells

Short hairpin RNAs (shRNAs) were designed and synthesized by GeneChem Co., Ltd. (Shanghai, China). The shRNA-control vector and shRNA-SLC1A5 or shRNA-MYC were transfected into H1299 and A549 cells using Lipofectamine 2000 transfection reagent (Invitrogen, Carlsbad, CA, USA). Cells were infected with lentivirus for 48 h and then selected with 2 ng/ml puromycin for 2 weeks, refreshing the medium every 3 days.

Cell proliferation

Cell proliferation was measured by the cell counting kit-8 (CCK-8) and 5-ethynyl-2'-deoxyuridine (EdU) incorporation. Cells (5×10^3) were seeded in 96-well plates, and the recommended volume of CCK-8 solution was added at 24, 48, and 72 h, respectively. The EdU incorporation assay was performed using an EdU Incorporation kit, following the instructions. Briefly, cells were inoculated in 96-well plates (3×10^3), cultured in 60% oxygen for 24 h, and incubated in EdU at a concentration of 50 μM for 2 h. Cells were then fixed and stained with Apollo dye (which reacts with EdU to detect it). Ultimately, cell nuclei were

stained with Hoechst33342.

Cell invasion, migration, and wound healing assays

For the migration assay, H1299, A549, H226 and LLC cells ($2\sim4\times10^4$) were seeded in serum-free medium in the upper chamber and cultured in 60% oxygen for 24 h. For the invasion assay, the Transwell filter inserts were coated with Matrigel, and 1×10^5 cells were seeded in serum-free medium in the upper chamber and in 60% oxygen for 24 h. Cancer cells that traversed the membrane were stained with crystal violet (0.04%) and counted.

Analysis of cell apoptosis

The Annexin V fluorescein isothiocyanate (FITC) / propidium iodide (PI) apoptosis detection kit (KeyGen Biotech Co., Ltd., Nanjing, China) was used for the detection of apoptotic cells with corresponding treatment.

RNA extraction, reverse transcription, and qRT-PCR analysis

RNA was extracted with TRIzol (Invitrogen) and cDNA was synthesized according to the method described in the HiScript First Strand cDNA synthesis kit (Vazyme Biotech Co., Ltd., Nanjing, China). The qRT-qPCR analysis was performed according to the procedure described in the UltraSYBR one-step RT-qPCR kit (CWBIO, Beijing, China). The primers used for qRT-PCR analysis are listed in Supplementary Table 1.

Western blot analysis

Cells were lysed using the Cell Total Protein Extraction Kit (Sangon Biotech, Shanghai, China) for whole cell lysate. Total protein was separated by sodium dodecyl sulfate-polyacrylamide gel electrophoresis (SDS-PAGE) and transferred to 0.45 μm polyvinylidene fluoride (PVDF) membranes (MilliporeSigma, Burlington, MA, USA). After blocking with 5%

non-fat milk for 1 h, primary antibodies against SLC1A4, SLC1A5, c-MYC, TBX4, TBX15, BACH1, HK2, PFK2, MCT1, GPI, HIF1α, GAPDH and Tubulin were separately incubated with the membranes at 4 °C overnight. Subsequently, the membranes were incubated with the corresponding secondary antibody for 1 h at room temperature. Eventually, the immunoreacted protein bands were visualized. The anti-body used in this study are listed in Supplementary Table 3.

Enzyme-linked immunosorbent assay (ELISA)

To detect intracellular glutamine and glutathione, cells were incubated overnight under normal conditions, followed by a change to fresh medium and continued incubation at 21% oxygen and 60% oxygen for 12, 24, and 48 h. The culture medium was removed and cells were rinsed with PBS before adding the appropriate amount of lysis buffer to obtain the cell lysate. Then, the cell lysate was centrifuged at 10,000-14,000g for 3-5 minutes and the supernatant was collected and used in subsequent measurements as described in the kit.

Glutamine uptake

The day before 60% O_2 exposure, H1299 and A549 cells were seeded in 24-well plates at a density of 5×10^4 cells/well and incubated in a normal incubator (21% O_2) or a 60% hyperoxia incubator for 24 h. H1299 and A549 cells with or without shSlc1a5 treatment were seeded in 24-well paltes at a density of 5×10^4 cells/well and incubated in a normal incubator for 24h. Cells were then washed twice with PBS and fresh medium containing [^{14}C]-glutamine (glutamine concentration of 4 mM) was added for 15 min. Background cells as well as counting wells (normalized) were added with normal medium and test wells were added with radiolabeled medium. Then, cells were lysed with 1% SDS and lysis products

were counted using a scintillation counter.

Extracellular flux measurements

The extracellular acidification rate (ECAR) and oxygen consumption rate (OCR) were determined using an Agilent Seahorse XFe96 extracellular flux analyzer (Agilent Technologies Inc.) as described in the manufacturer's protocol. Cells were seeded in 96-well microplates the day before the experiment and incubated in a normal incubator or a 60% hyperoxia incubator for 12 h. The hydrated probe plates were placed in a CO_2-free incubator overnight. Glucose (10 mM), oligomycin (1 mM) and 2-Deoxy-d-glucose (2-DG; 50 mM) were added successively to conduct the glycolytic stress test. Oligomycin (1.5 mM), carbonyl cyanide-p-trifluoromethoxyphenylhydrazone (FCCP; 1 mM) and rotenone and antimycin A (0.5 mM) were added successively to conduct the mitochondrial stress test.

Immunohistochemical (IHC) staining

The tissues microarrays were blocked with goat serum for 30 min before adding the primary antibody. Specimens were incubated with primary anti-SLC1A5 antibody for 12 h at 4 °C. Eventually, the microarrays were stained with 3, 3-diaminobenzidine solution and hematoxylin. The slides were photographed with an inverted microscope (Olympus Corporation, Tokyo, Japan).

Two pathologists separately assessed the specimens under blinded experimental conditions. The expression levels of SLC1A5 were evaluated by combining the percentage of cells with the staining intensity. The intensity of immunoreacted SLC1A5 was scored using a 0-3 scale (0, negative; 1, weak; 2, moderate; 3, strong); the percentage of immunoreactivity cells was graded as 1 (0-25%), 2 (26-50%), 3 (51-75%) and 4 (76-100%).

The staining index value (values, 0-12) was determined by multiplying the score for staining intensity by the score for the positive area. For statistical analysis, the level of SLC1A5 expression was categorized as low (0-4), middle (4-8) and high (8-12) expression.

Chromatin immunoprecipitation (ChIP) analysis

Cells were cultured under normal conditions for 24 h and chromatin immunoprecipitation ChIP Assay was performed using a ChiP assay kit (Beyond) using the procedure described by the manufacturer of the kit. Cells ($1x10^6$) were fixed in 1% formaldehyde for 10 min. Nuclei extracts were sonicated to fragment DNA to 200-1000bp. The fragmented chromatin obtained was divided into two ChiP reactions (C-MYC or control IgG). DNA was enriched by immunoprecipitation using 4 mg of anti-C-MYC or normal rabbit IgG control antibody complexed with protein A agarose beads. Protein K treatment removed the protein and unenriched DNA samples were treated in the same way as control input. PCR was performed on the CHIP and input DNA using primers for the SLC1A5 promoter region containing the MYC binding site.

Luciferase reporter assay

The luciferase reporter assay was performed according to a previous report[46]. Briefly, the luciferase reporter vector was constructed using 0.5 μg of pGL3 plasmid containing the putative MYC binding site or response element or its mutant. The constructed luciferase reporter vector was transiently co-transfected in triplicate into 293T cells. The Dual Luciferase Kit (Promega Corporation, Madison, WI, USA) was used to determine the luciferase activity. Firefly luciferase activity was normalized to the Renilla luciferase control value and shown as the average of triplicate measurements.

Quantification and statistical analysis

The statistical analyses were performed using GraphPad Prism 8.0.1 (GraphPad Software Inc., San Diego, CA, USA). Values are presented as the mean ± SEM unless stated otherwise. Details of the specific statistical analysis are indicated in the figure legends.

References

1. Hoadley KA, Yau C, Hinoue T, Wolf DM, Lazar AJ, Drill E, Shen R, Taylor AM, Cherniack AD, Thorsson V, Akbani R, Bowlby R, Wong CK, Wiznerowicz M, Sanchez-Vega F, Robertson AG, Schneider BG, Lawrence MS, Noushmehr H, Malta TM, Cancer Genome Atlas N, Stuart JM, Benz CC, Laird PW. Cell-of-Origin Patterns Dominate the Molecular Classification of 10,000 Tumors from 33 Types of Cancer. *Cell* 2018: 173(2): 291-304 e296.
2. Klemm F, Maas RR, Bowman RL, Kornete M, Soukup K, Nassiri S, Brouland JP, Iacobuzio-Donahue CA, Brennan C, Tabar V, Gutin PH, Daniel RT, Hegi ME, Joyce JA. Interrogation of the Microenvironmental Landscape in Brain Tumors Reveals Disease-Specific Alterations of Immune Cells. *Cell* 2020: 181(7): 1643-1660 e1617.
3. Faubert B, Solmonson A, DeBerardinis RJ. Metabolic reprogramming and cancer progression. *Science* 2020: 368(6487).
4. Guha P, Gardell J, Rabinowitz B, Lopes M, DaSilva NA, Rowley D, Katz SC. Monocytic and granulocytic myeloid-derived suppressor cell plasticity and differentiation are organ-specific. *Oncogene* 2021: 40(3): 693-704.
5. Zhang C, Yu D. Suppressing immunotherapy by organ-specific tumor microenvironments: what is in the brain? *Cell & bioscience* 2019: 9: 82.
6. Schulz M, Salamero-Boix A, Niesel K, Alekseeva T, Sevenich L. Microenvironmental Regulation of Tumor Progression and Therapeutic Response in Brain Metastasis. *Frontiers in immunology* 2019: 10: 1713.
7. Quail DF, Joyce JA. Microenvironmental regulation of tumor progression and metastasis. *Nature medicine* 2013: 19(11): 1423-1437.
8. Schwarte LA, Schober P, Loer SA. Benefits and harms of increased inspiratory oxygen concentrations. *Current opinion in anaesthesiology* 2019: 32(6): 783-791.
9. Kim SW, Kim IK, Ha JH, Yeo CD, Kang HH, Kim JW, Lee SH. Normobaric hyperoxia inhibits the progression of lung cancer by inducing apoptosis. *Experimental biology and medicine* 2018: 243(9): 739-748.
10. Schumann M, Schulz H, Hackney AC, Bloch W. Feasibility of high-intensity interval training with hyperoxia vs. intermittent hyperoxia and hypoxia in cancer patients undergoing chemotherapy - Study protocol of a randomized controlled trial. *Contemporary clinical trials communications* 2017: 8: 213-217.
11. Al-Waili NS, Butler GJ. Effects of hyperbaric oxygen on inflammatory response to wound and trauma: possible mechanism of action. *TheScientificWorldJournal* 2006: 6: 425-441.
12. Hatfield SM, Kjaergaard J, Lukashev D, Schreiber TH, Belikoff B, Abbott R, Sethumadhavan S,

Philbrook P, Ko K, Cannici R, Thayer M, Rodig S, Kutok JL, Jackson EK, Karger B, Podack ER, Ohta A, Sitkovsky MV. Immunological mechanisms of the antitumor effects of supplemental oxygenation. *Science translational medicine* 2015: 7(277): 277ra230.

13. Pavlova NN, Thompson CB. The Emerging Hallmarks of Cancer Metabolism. *Cell metabolism* 2016: 23(1): 27-47.

14. DeBerardinis RJ, Chandel NS. Fundamentals of cancer metabolism. *Science advances* 2016: 2(5): e1600200.

15. Wise DR, DeBerardinis RJ, Mancuso A, Sayed N, Zhang XY, Pfeiffer HK, Nissim I, Daikhin E, Yudkoff M, McMahon SB, Thompson CB. Myc regulates a transcriptional program that stimulates mitochondrial glutaminolysis and leads to glutamine addiction. *Proceedings of the National Academy of Sciences of the United States of America* 2008: 105(48): 18782-18787.

16. Wiel C, Le Gal K, Ibrahim MX, Jahangir CA, Kashif M, Yao H, Ziegler DV, Xu X, Ghosh T, Mondal T, Kanduri C, Lindahl P, Sayin VI, Bergo MO. BACH1 Stabilization by Antioxidants Stimulates Lung Cancer Metastasis. *Cell* 2019: 178(2): 330-345 e322.

17. Ou Y, Wang SJ, Li D, Chu B, Gu W. Activation of SAT1 engages polyamine metabolism with p53-mediated ferroptotic responses. *Proceedings of the National Academy of Sciences of the United States of America* 2016: 113(44): E6806-E6812.

18. Ma T, Patel H, Babapoor-Farrokhran S, Franklin R, Semenza GL, Sodhi A, Montaner S. KSHV induces aerobic glycolysis and angiogenesis through HIF-1-dependent upregulation of pyruvate kinase 2 in Kaposi's sarcoma. *Angiogenesis* 2015: 18(4): 477-488.

19. Yuneva MO, Fan TW, Allen TD, Higashi RM, Ferraris DV, Tsukamoto T, Mates JM, Alonso FJ, Wang C, Seo Y, Chen X, Bishop JM. The metabolic profile of tumors depends on both the responsible genetic lesion and tissue type. *Cell metabolism* 2012: 15(2): 157-170.

20. Morishita A, Zaidi MR, Mitoro A, Sankarasharma D, Szabolcs M, Okada Y, D'Armiento J, Chada K. HMGA2 is a driver of tumor metastasis. *Cancer research* 2013: 73(14): 4289-4299.

21. Zheng G, Ma Y, Zou Y, Yin A, Li W, Dong D. HCMDB: the human cancer metastasis database. *Nucleic acids research* 2018: 46(D1): D950-D955.

22. Feng S, Zhang L, Liu X, Li G, Zhang B, Wang Z, Zhang H, Ma H. Low levels of AMPK promote epithelial-mesenchymal transition in lung cancer primarily through HDAC4- and HDAC5-mediated metabolic reprogramming. *Journal of cellular and molecular medicine* 2020: 24(14): 7789-7801.

23. Kim TH, Kim E, Yoon D, Kim J, Rhim TY, Kim SS. Recombinant human prothrombin kringles have potent anti-angiogenic activities and inhibit Lewis lung carcinoma tumor growth and metastases. *Angiogenesis* 2002: 5(3): 191-201.

24. Wang X, Adjei AA. Lung cancer and metastasis: new opportunities and challenges. *Cancer metastasis reviews* 2015: 34(2): 169-171.

25. Tompach PC, Lew D, Stoll JL. Cell response to hyperbaric oxygen treatment. *International journal of oral and maxillofacial surgery* 1997: 26(2): 82-86.

26. Villacampa P, Liyanage SE, Klaska IP, Cristante E, Menger KE, Sampson RD, Barlow M, Abelleira-Hervas L, Duran Y, Smith AJ, Ali RR, Luhmann UFO, Bainbridge JWB. Stabilization of myeloid-derived HIFs promotes vascular regeneration in retinal ischemia. *Angiogenesis* 2020: 23(2): 83-90.

27. Liu ZJ, Velazquez OC. Hyperoxia, endothelial progenitor cell mobilization, and diabetic wound healing. *Antioxidants & redox signaling* 2008: 10(11): 1869-1882.

28. Fosen KM, Thom SR. Hyperbaric oxygen, vasculogenic stem cells, and wound healing. *Antioxidants & redox signaling* 2014: 21(11): 1634-1647.

29. Wenwu L, Xuejun S, Hengyi T, Kan L. Hyperbaric oxygen and cancer: more complex than we expected. *Targeted oncology* 2013: 8(2): 79-81.
30. Bennett M, Feldmeier J, Smee R, Milross C. Hyperbaric oxygenation for tumour sensitisation to radiotherapy. *The Cochrane database of systematic reviews* 2005(4): CD005007.
31. Heys SD, Smith IC, Ross JA, Gilbert FJ, Brooks J, Semple S, Miller ID, Hutcheon A, Sarkar T, Eremin O. A pilot study with long term follow up of hyperbaric oxygen pretreatment in patients with locally advanced breast cancer undergoing neo-adjuvant chemotherapy. *Undersea & hyperbaric medicine : journal of the Undersea and Hyperbaric Medical Society, Inc* 2006: 33(1): 33-43.
32. Baish JW, Gazit Y, Berk DA, Nozue M, Baxter LT, Jain RK. Role of tumor vascular architecture in nutrient and drug delivery: an invasion percolation-based network model. *Microvascular research* 1996: 51(3): 327-346.
33. Steingold JM, Hatfield SM. Targeting Hypoxia-A2A Adenosinergic Immunosuppression of Antitumor T Cells During Cancer Immunotherapy. *Frontiers in immunology* 2020: 11: 570041.
34. Halpin-Veszeleiova K, Hatfield SM. Oxygenation and A2AR blockade to eliminate hypoxia/HIF-1alpha-adenosinergic immunosuppressive axis and improve cancer immunotherapy. *Current opinion in pharmacology* 2020: 53: 84-90.
35. Son J, Lyssiotis CA, Ying H, Wang X, Hua S, Ligorio M, Perera RM, Ferrone CR, Mullarky E, Shyh-Chang N, Kang Y, Fleming JB, Bardeesy N, Asara JM, Haigis MC, DePinho RA, Cantley LC, Kimmelman AC. Glutamine supports pancreatic cancer growth through a KRAS-regulated metabolic pathway. *Nature* 2013: 496(7443): 101-105.
36. Yang S, Hwang S, Kim M, Seo SB, Lee JH, Jeong SM. Mitochondrial glutamine metabolism via GOT2 supports pancreatic cancer growth through senescence inhibition. *Cell death & disease* 2018: 9(2): 55.
37. Momcilovic M, Bailey ST, Lee JT, Fishbein MC, Braas D, Go J, Graeber TG, Parlati F, Demo S, Li R, Walser TC, Gricowski M, Shuman R, Ibarra J, Fridman D, Phelps ME, Badran K, St John M, Bernthal NM, Federman N, Yanagawa J, Dubinett SM, Sadeghi S, Christofk HR, Shackelford DB. The GSK3 Signaling Axis Regulates Adaptive Glutamine Metabolism in Lung Squamous Cell Carcinoma. *Cancer cell* 2018: 33(5): 905-921 e905.
38. Wolfer A, Ramaswamy S. MYC and metastasis. *Cancer research* 2011: 71(6): 2034-2037.
39. Romero OA, Torres-Diz M, Pros E, Savola S, Gomez A, Moran S, Saez C, Iwakawa R, Villanueva A, Montuenga LM, Kohno T, Yokota J, Sanchez-Cespedes M. MAX inactivation in small cell lung cancer disrupts MYC-SWI/SNF programs and is synthetic lethal with BRG1. *Cancer discovery* 2014: 4(3): 292-303.
40. Wolfer A, Wittner BS, Irimia D, Flavin RJ, Lupien M, Gunawardane RN, Meyer CA, Lightcap ES, Tamayo P, Mesirov JP, Liu XS, Shioda T, Toner M, Loda M, Brown M, Brugge JS, Ramaswamy S. MYC regulation of a "poor-prognosis" metastatic cancer cell state. *Proceedings of the National Academy of Sciences of the United States of America* 2010: 107(8): 3698-3703.
41. Le Gal K, Ibrahim MX, Wiel C, Sayin VI, Akula MK, Karlsson C, Dalin MG, Akyurek LM, Lindahl P, Nilsson J, Bergo MO. Antioxidants can increase melanoma metastasis in mice. *Science translational medicine* 2015: 7(308): 308re308.
42. Wang H, Liu X, Long M, Huang Y, Zhang L, Zhang R, Zheng Y, Liao X, Wang Y, Liao Q, Li W, Tang Z, Tong Q, Wang X, Fang F, Rojo de la Vega M, Ouyang Q, Zhang DD, Yu S, Zheng H. NRF2 activation by antioxidant antidiabetic agents accelerates tumor metastasis. *Science translational medicine* 2016: 8(334): 334ra351.
43. Piskounova E, Agathocleous M, Murphy MM, Hu Z, Huddlestun SE, Zhao Z, Leitch AM, Johnson TM,

DeBerardinis RJ, Morrison SJ. Oxidative stress inhibits distant metastasis by human melanoma cells. *Nature* 2015: 527(7577): 186-191.

44. Lee HY, Kim IK, Lee HI, Lee HY, Kang HS, Yeo CD, Kang HH, Moon HS, Lee SH. Combination of carboplatin and intermittent normobaric hyperoxia synergistically suppresses benzo[a]pyrene-induced lung cancer. *The Korean journal of internal medicine* 2018: 33(3): 541-551.

45. Justilien V, Fields AP. Utility and applications of orthotopic models of human non-small cell lung cancer (NSCLC) for the evaluation of novel and emerging cancer therapeutics. *Current protocols in pharmacology* 2013: 62: 14 27 11-14 27 17.

46. Yue M, Jiang J, Gao P, Liu H, Qing G. Oncogenic MYC Activates a Feedforward Regulatory Loop Promoting Essential Amino Acid Metabolism and Tumorigenesis. *Cell reports* 2017: 21(13): 3819-3832.

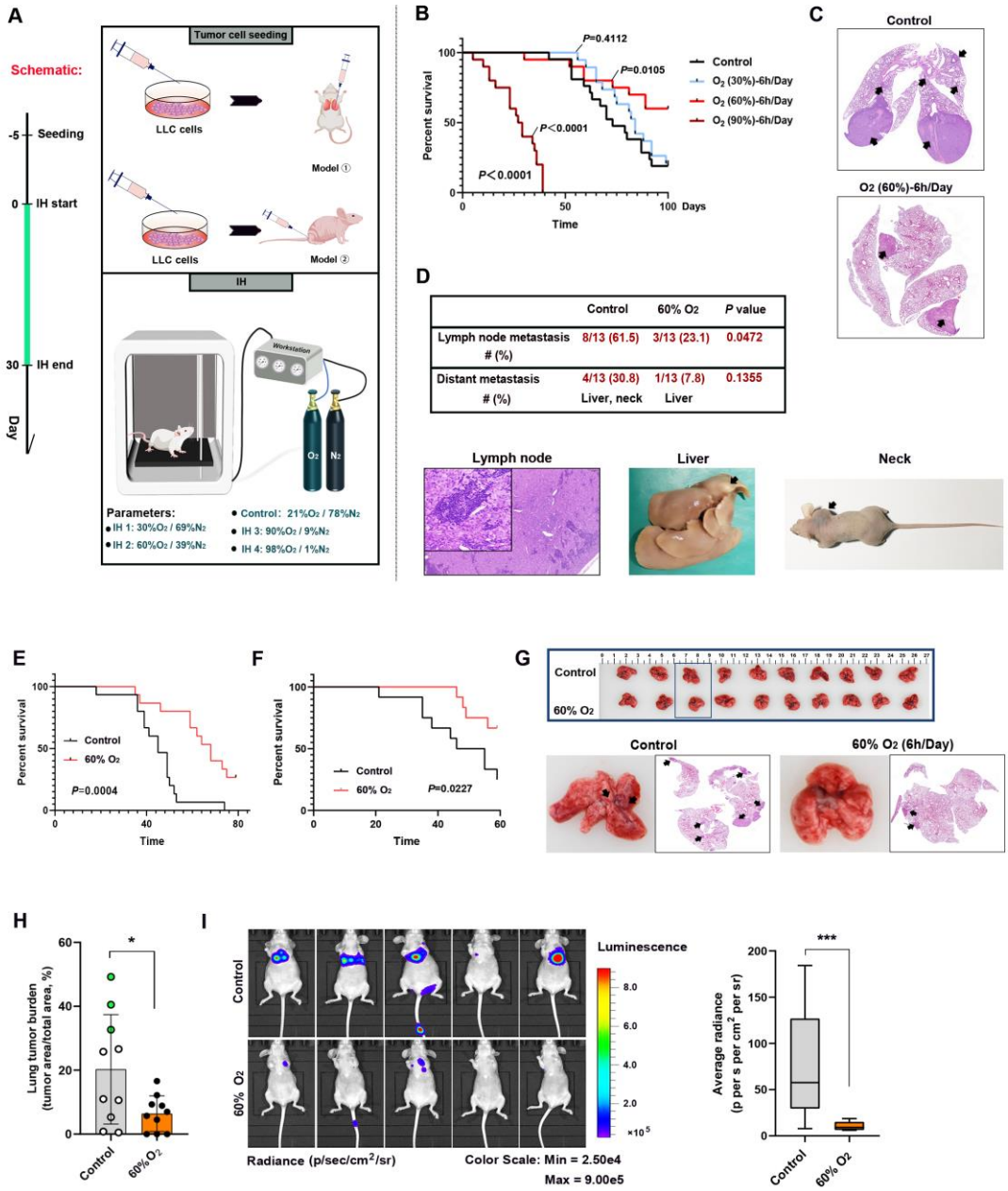

Figure 1. Inspiratory hyperoxia suppresses lung cancer metastasis.

(A) Schematic of the workflow for the establishment of lung cancer models and IH

treatment.

(B) Effects of IH treatment (30% O_2, 60% O_2, 90% O_2) on the long-term survival in the orthotopic lung tumor models (n=15). Statistical significance was calculated using a log-rank test.

(C) Representative lung sections, arrows indicate lung tumors.

(D) Percentage of mice with lymph node metastasis and distant metastasis and representative images, Chi-square test.

(E) Sixty percent oxygen treatment leads to long-term survival in the lung metastasis models with LLC cells i.v. injection (n=15), log-rank test.

(F) Sixty percent oxygen treatment leads to long-term survival in the lung metastasis models with H1299 cells i.v. injection (n=15), log-rank test.

(G) Representative lung photos and lung sections of tumor-bearing mice.

(H) IH decreases lung tumor burden in mice four weeks after i.v. injection of H1299 cells (n=10), green dot indicats mice with distant metastasis.

(I) Left, bioluminescence imaging four weeks after injection into mice via tail vein. Right, box plot (n=5), *$P<0.05$, ***$P<0.001$ vs the indicated group, two-tailed Student's t-test.

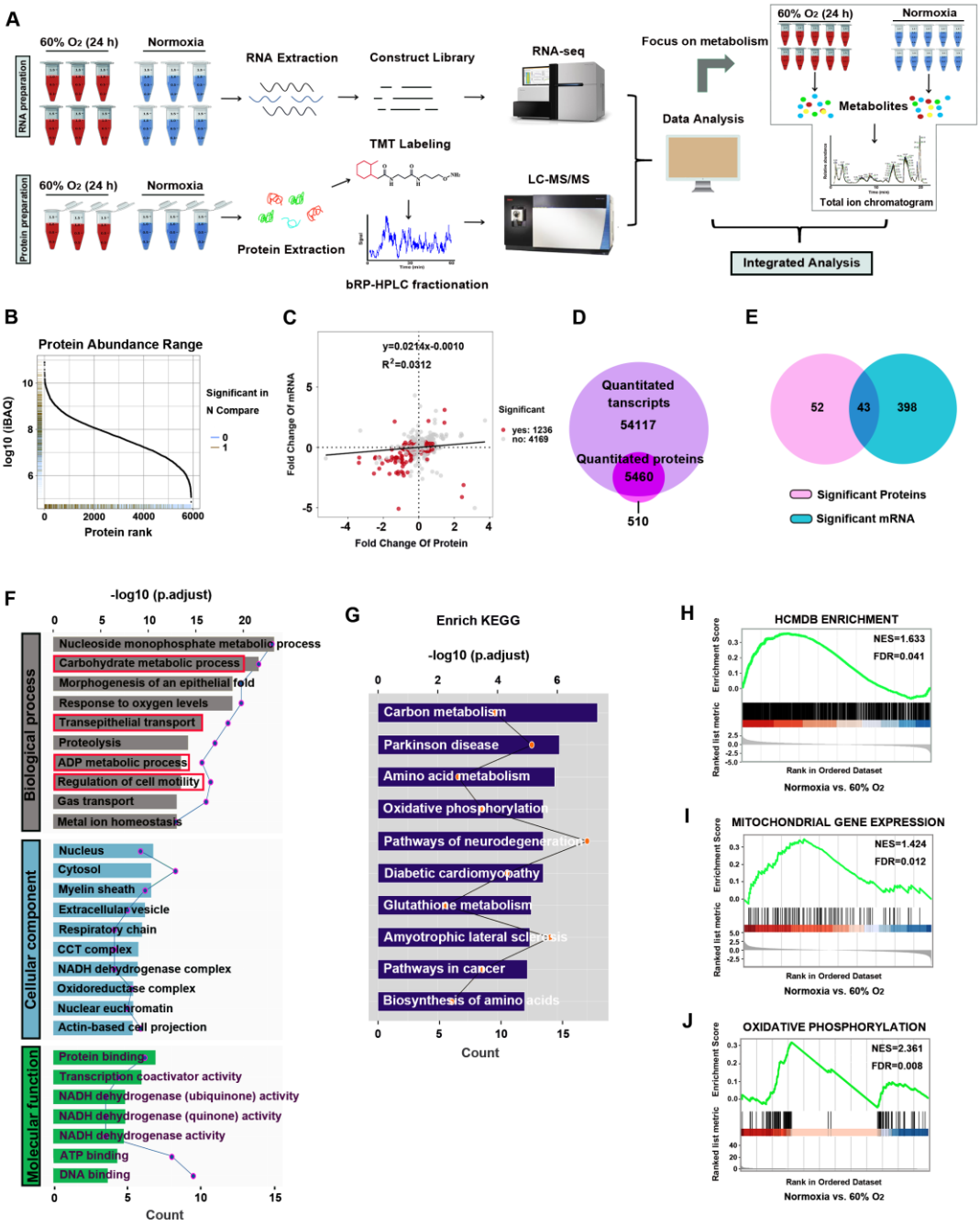

Figure 2. Multi-omics data of H1299 cells treated with hyperoxia.

(A) Schematic diagram of the workflow for the analysis of the transcriptome, proteome and metabolome.

(B) Dynamic range of protein expression.

(C) Scatter plot of the correlation between genes quantified in both transcriptomic and proteomic datasets.

(D) Venn diagram showing the number of identified mRNAs and proteins by RNA-seq and LC-MS/MS.

(E) Venn diagram showing significantly enriched mRNAs (fold change (FC) ≥ 2; false-discovery rate (FDR) < 0.05) and proteins (FC ≥ 2; FDR < 0.05), and their overlap.

(F) GO enrichment analysis is used to classify the significant differentially expressed mRNAs and proteins.

(G) KEGG enrichment analysis of the significant differentially expressed mRNAs and proteins.

(H) Upregulation of HCMDB genes in 60% O_2 (24 h) treated H1299 cells *vs.* controls.

(I, J) Gene set enrichment analysis of significant differentially expressed mRNAs with normalized enrichment score (NES) and false-discovery rate (FDR) Q value.

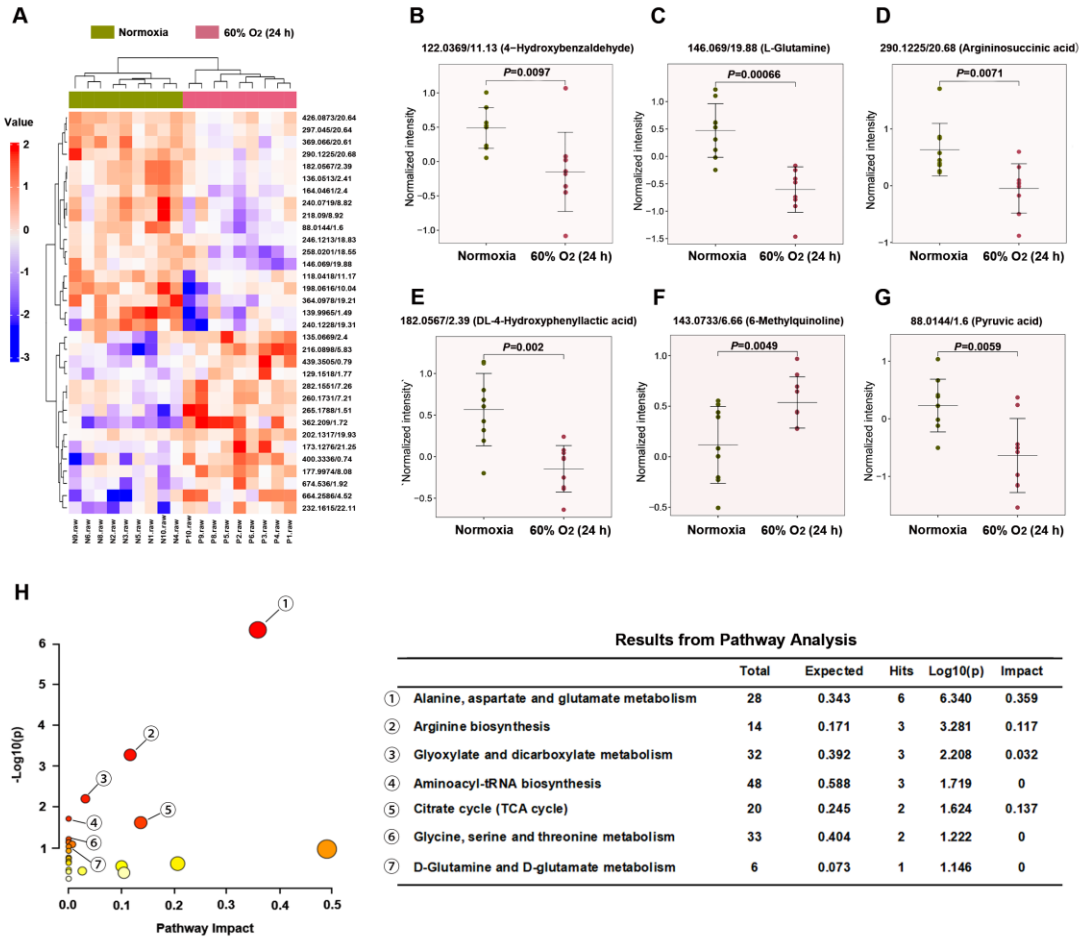

Results from Pathway Analysis

		Total	Expected	Hits	Log10(p)	Impact
①	Alanine, aspartate and glutamate metabolism	28	0.343	6	6.340	0.359
②	Arginine biosynthesis	14	0.171	3	3.281	0.117
③	Glyoxylate and dicarboxylate metabolism	32	0.392	3	2.208	0.032
④	Aminoacyl-tRNA biosynthesis	48	0.588	3	1.719	0
⑤	Citrate cycle (TCA cycle)	20	0.245	2	1.624	0.137
⑥	Glycine, serine and threonine metabolism	33	0.404	2	1.222	0
⑦	D-Glutamine and D-glutamate metabolism	6	0.073	1	1.146	0

Figure 3. Metabolic profiles with metabolite compositions and metabolic pathways.

(A) Heat map analysis of metabolite compositions between 60% O_2 (24 h) and normoxia groups.

(B-G) Quantitation of the levels of 6-methylquinoline, argininosuccinic acid, DL-4-hydroxyphenyllactic acid, 4-hydroxybenzaldehyde, L-glutamine and pyruvic acid, two-tailed Student's t-test.

(H) The metabolic pathways identified using MetaboAnalyst 3.0 software.

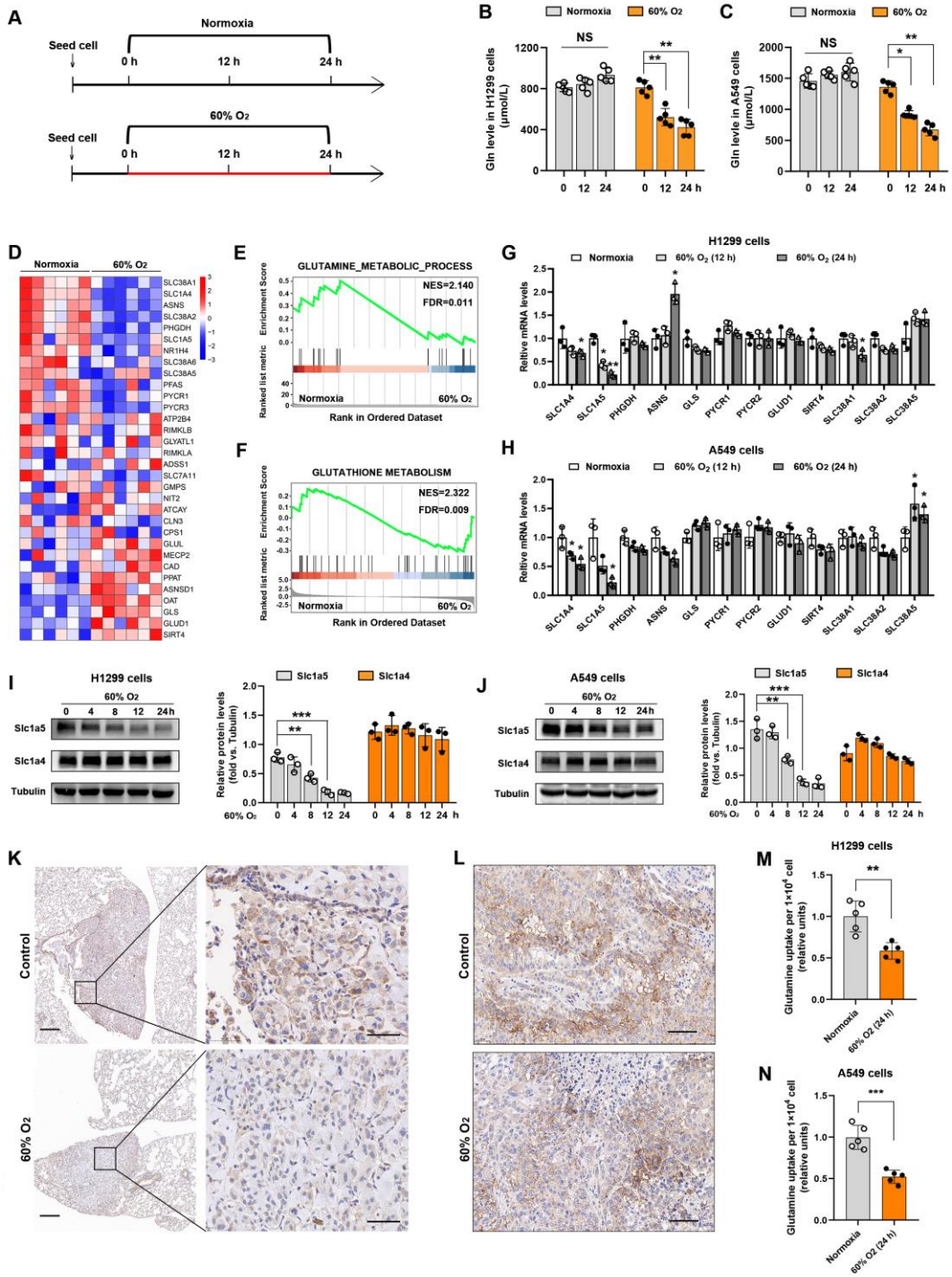

Figure 4. Inspiratory hyperoxia decreases the glutamine uptake in lung tumors.

(A) Schematic diagram of the workflow for the measurement of intracellular glutamine levels. The red line indicates that the cells that were cultured in 60% O_2, and the black line

indicates that the cells that were cultured in 21% O_2.

(B, C) Hyperoxia treatment decreases the level of glutamine in H1299 and A549 cells (n=5), one-way ANOVA followed by the Tukey's post hoc test.

(D) Heat map depicting changes in the expression of genes involved in "glutamine metabolism" between 60% O_2 (24 h) and normoxia group.

(E, F) GSEA results indicate that genes related to "glutamine metabolic process" (E) and "glutathione metabolism" (F) are differentially enriched in H1299 cells cultured in normoxia and 60% O_2 (24 h). NES, normalized enrichment score. FDR, false-discovery rate.

(G, H) The levels of glutamine metabolism related genes are determined by qRT-PCR in H1299 and A549 cells (n=3).

(I, J) Western blot analysis for the expressions of SLC1A4 and SLC1A5 in H1299 and A549 cells (n=3), one-way ANOVA followed by the Tukey's post hoc test.

(K) IH treatment reduces the expression of SLC1A5 in lung tumor in lung metastasis models, bar (left)=200 μm, bar (right)=50 μm.

(L) IHC staining for the expression of SLC1A5 in xenograft tumors, bar=50 μm.

(M, N) Effect of 60% O_2 (24 h) treatment on the relative glutamine uptake in H1299 and A549 cells (n=5).

*$P<0.05$, **$P<0.01$, ***$P<0.001$, NS, $P>0.05$ vs the normoxia or indicated group, two-tailed Student's t-test.

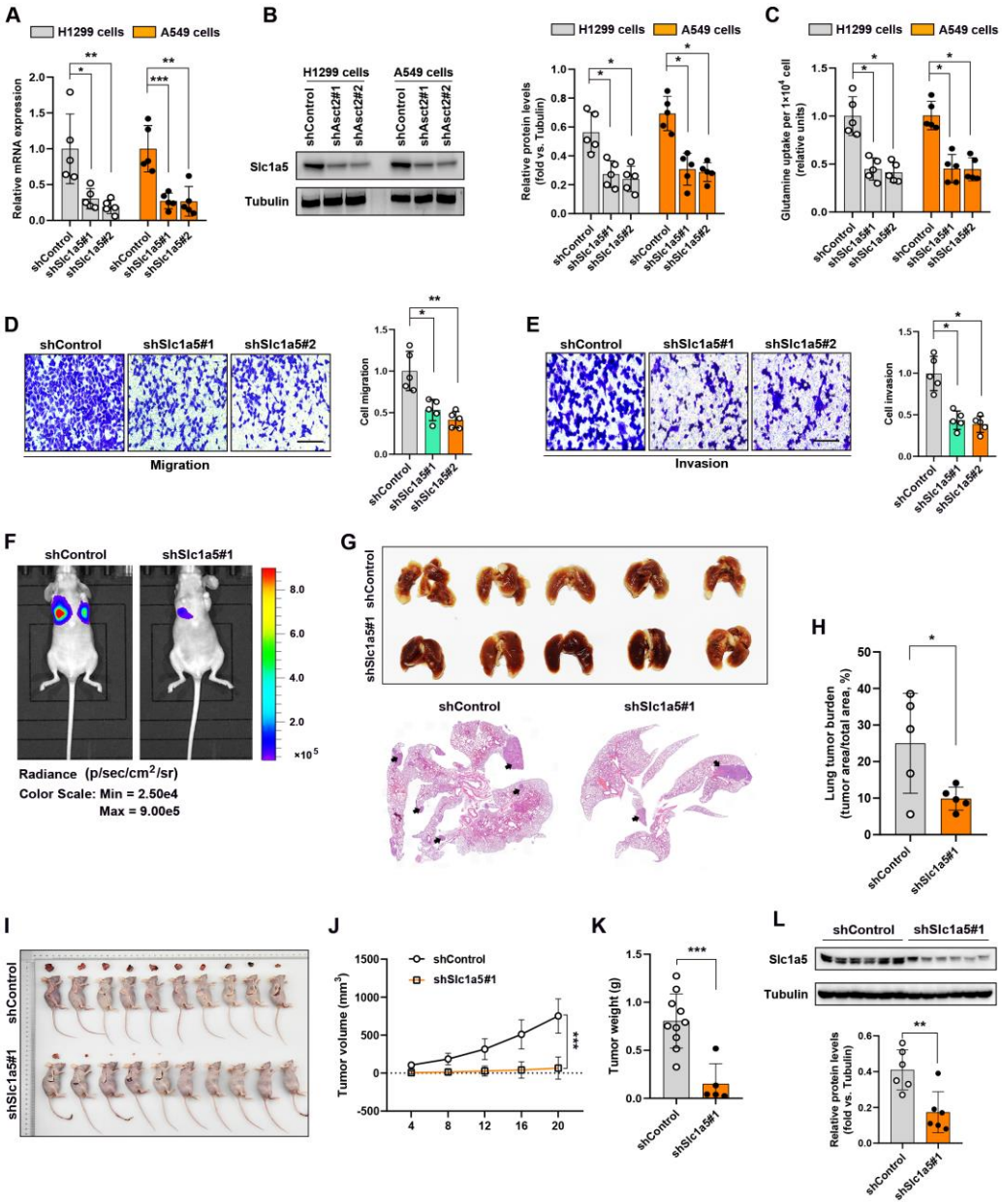

Figure 5. SLC1A5 mediates the hyperoxia-induced suppression of glutamine catabolism.

(A, B) Knockdown of SLC1A5 is confirmed at the mRNA and protein level in H1299 and

A549 cells (n=5).

(C) Determination of the relative glutamine uptake in H1299 and A549 cells with shSLC1A5 treatment (n=5).

(D, E) The migration and invasion of H1299 cells (12 h) with shControl and shSLC1A5 treatment (n=5), bar=50 μm.

(F) Representative bioluminescence images of mice four weeks after i.v. injection of H1299 cells.

(G, H) Lung tumor burden in mice four weeks after i.v. injection of H1299 cells and representative lung section (n=5).

(I-K) Photographs of Matrigel plugs excised from mice after 21 days of growth in vivo and quantitative analysis of the tumor volume and tumor weight (n=10).

(L) Detection of SLC1A5 expressions in xenograft models by Western blot analysis (n=6).

*$P<0.05$, **$P<0.01$, ***$P<0.001$ vs the indicated group, two-tailed Student's t-test.

1

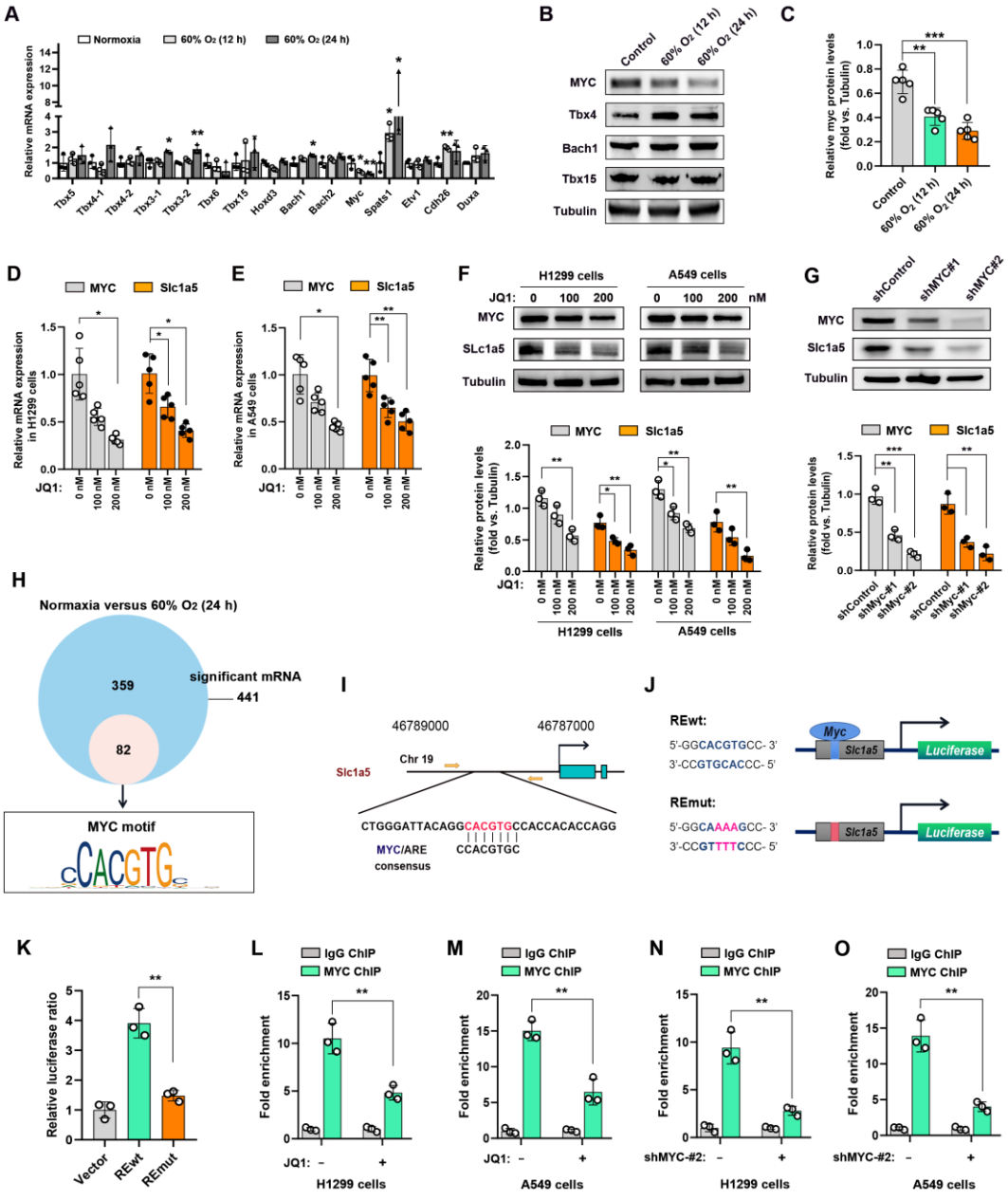

Figure 6. MYC directly activates SLC1A5 transcription.

(A) qRT-PCR analysis is used to determine the levels of transcription factors with

significant differences identified by RNA-seq in H1299 cellls (n=3).

(B, C) Western blots analysis showing that exposure to 60% O_2 for 12 h and 24 h results in a decrease in MYC protein expression in H1299 cells (n=5).

(D-F) Analysis of MYC and SLC1A5 expressions in H1299 and A549 cells treated with JQ1.

(G) Effect of MYC knockdown on the expression level of SLC1A5 protein in H1299 cells (n=3).

(H) Venn diagram of the RNA-seq data showing the number of genes differentially expressed in H1299 cells with 60% O_2 treatment *vs.* the control cells (blue). Small circle show genes with MYC binding motifs in their proximal promoter.

(I) Predicted binding site MYC-binding sites of SLC1A5. Yellow arrows show primers used for ChIP-qPCR analysis.

(J) Schematic of the MYC binding site, the MYC response elements (MYC REwt), and its mutants (REmut) within the promoter of SLC1A5.

(K) Luciferase activity of 293T cell with and without ectopically expressed MYC (n=3).

(L-O) Binding of MYC to SLC1A5 is analyzed by ChIP assays in H1299 and A549 cells with and without JQ1 and MYC knockdown treatment (n=3).

*$P<0.05$, **$P<0.01$, ***$P<0.001$ vs the normoxia or indicated group, two-tailed Student's t-test.

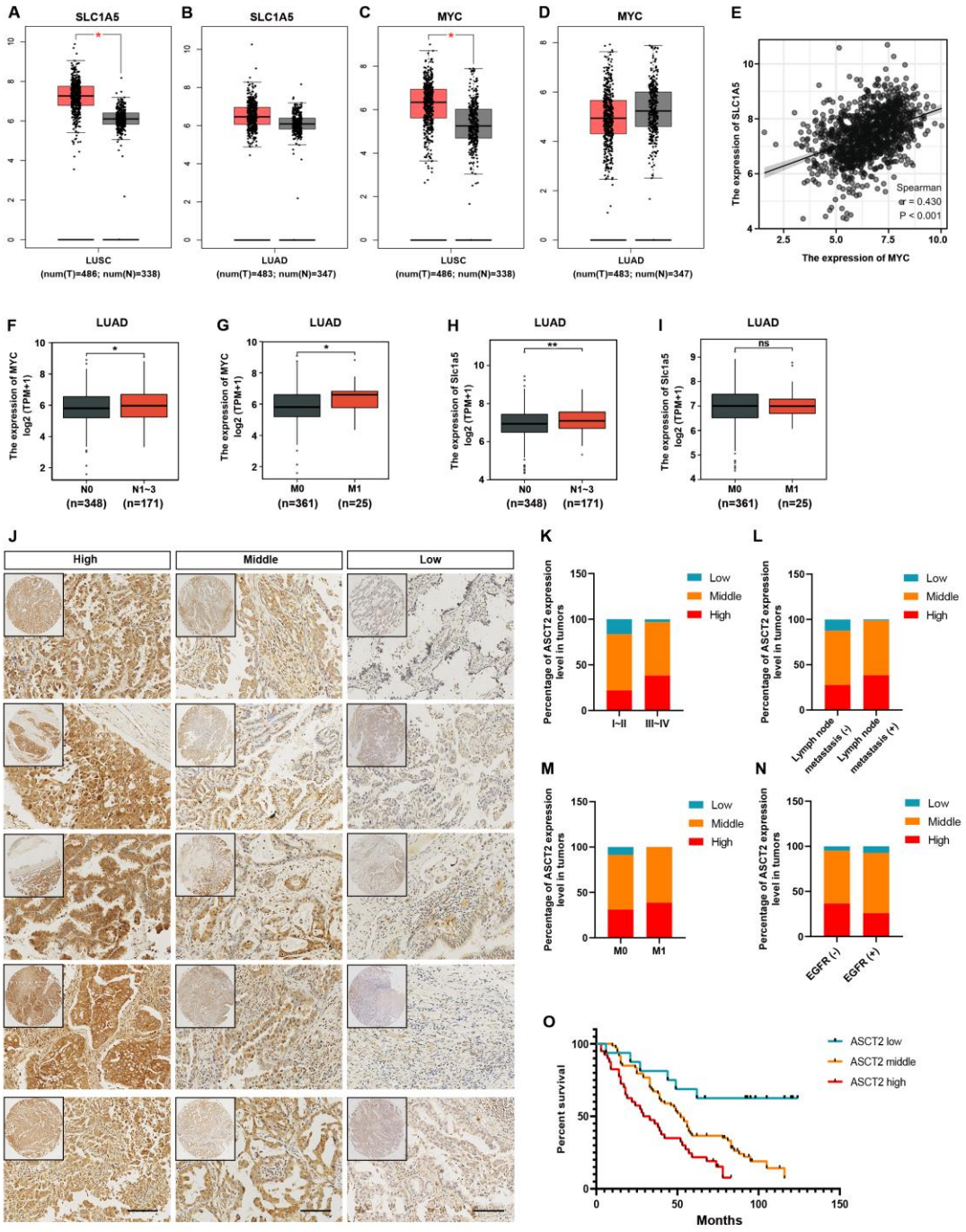

Figure 7. SLC1A5 is associated with the tumor stage, lymph node metastases and poor survival in human NSCLC.

(A-D) SLC1A5 and MYC expressions were analyzed in NSCLC tissues (n=969) and their

adjacent noncancerous tissues in the GEPIA database.

(E) Correlation between mRNA levels of SLC1A5 *vs.* MYC in NSCLC tissues according to TCGA database, r=0.430, $P<0.001$.

(F-I) Data of TCGA datasets showing that SLC1A5 is closely related to lymph node metastasis and distant metastasis in LUAD, $*P<0.05$, $**P<0.01$, NS, $P>0.05$ vs indicated group.

(J) Representative images from human NSCLC tumors stained with SLC1A5, bar=100 μm.

(K-N) Correlation of SLC1A5 expression with tumor grade, lymph node metastasis, distant metastasis and EGFR mutation in 219 NSCLC patients, Chi-square test.

(O) Kaplan–Meier survival curve analysis was performed to examine the effects of the genes on the survival rate in NSCLC ($P<0.001$), log-rank test.

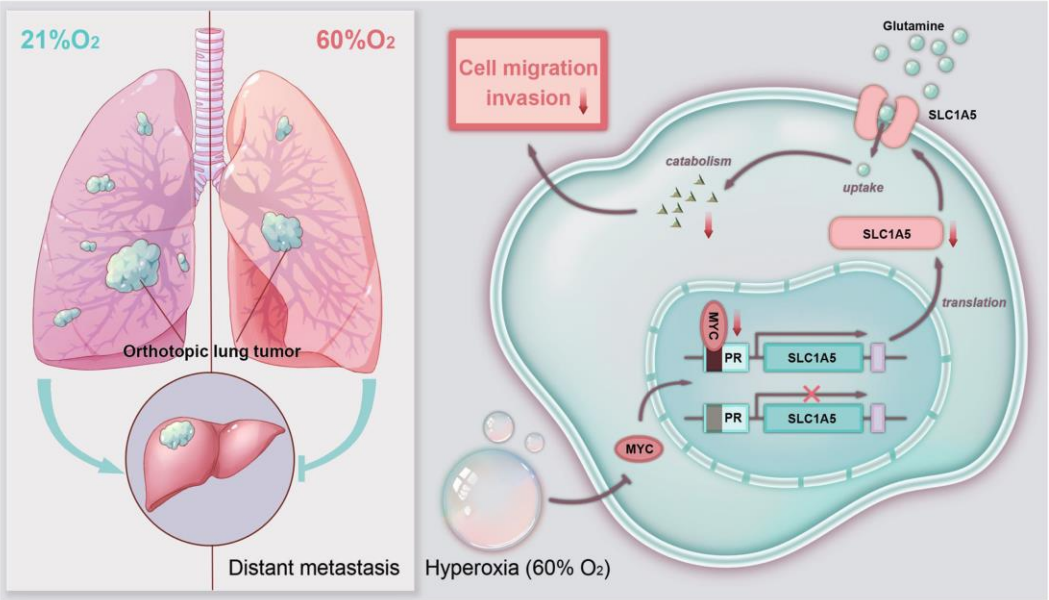

Figure 8. Graphical summary of the mechanism of IH supresses lung cancer metastasis through a MYC/SLC1A5-dependent metabolic pathway.

Hyperoxia treatment (60% O_2) reduces the expression level of MYC, resulting in down-regulation of the MYC target gene SLC1A5 in NSCLC cells. Low levels of SLC1A5 lead to disturbance in glutamine uptake and catabolism, ultimately leading to a reduction in lung cancer cell invasiveness and inhibition of metastasis. PR, promoter region.

Supplementary Table 1: Primer sequences used in this study

Gene	Forward (5'-3')	Reverse (5'-3')
TBX3-1	ACACTGGAAATGGCCGAAGA	GCTTGTTCACTGGAGGACTCA
TBX3-2	TCTGAAACCGACGTTCAGGAG	TGCACTTCAAAGGGAGGAGG
TBX4-1	GCATGAACCCCAAGACCAAG	CCCTGCCACCATCCATTTGT
TBX4-2	AGAACAATGCTTTCGGCTCCA	TCACGGGGTATTCTTTGCTCT
TBX5	CAGTTACAAAGTGAAGGTGACG	TGCGAATTTGTATCTGTGATCG
TBX6	CTATGGGAGCGGAGACACAC	CTCCTGGTGGGAAGGTGACT
TBX15	CCAACTTTTCATCTGGCCCC	CTCTGAAGCCTGTTGTAGCCA
BACH1	AAATGAATGCCTGGGAGGAGT	AATTGTGGGGGAAAGGAGTCA
BACH2	ATGGATTGCCAGAGCCTTCTCAT	TGCCGTTCACACCATGTAATTT
MYC	CTCCTACGTTGCGGTCACAC	GGTTCACCATGTCTCCTCCC
SPATS1	TTTAGCAGCAACATCCACACCTACC	AGCACTTGTCCACCGTCCTCTC
HOXD3	AGAGAGCTGCGAGGACAAGA	ACAAGTAGCGGTTGAAGTGGA
ETV1	TCTGGATACTGGCTACTGGCTACTG	AGGCTGGAGACAACAATGTGGAAG
CDH26	CTTAGGTGGCTGTTCTGGCGATG	GTGACACTGGTGACAATGAGGATGG
DUXA	GCATGGCCGAAGACACCTAT	TGTGTAACTGAGAGGCGCTG
SLC1A4	TGAGGCTTACCTCTCGGCA	CTGGACATGGATCAAGCCGAA
SLC1A5	GGTTACTCCTCAAAACCCCCA	GTGACCTGCTCCCTGAGACA
SLC38A1	GCATTTGTTTGCCACCCGTC	CGGACTGCACGTTGTCATAG
SLC38A2	AGATTTCAGTTGGTGGCGTC	TAACAGGAAGAACAAAGCCCCA
GLS	GTCCCGATTTGTGGGGTGT	GGACTGAAGACAGAAGGGAACT
GLUD1	TCAGCTATGGCCGTTTGACC	GCCGTGGGTACAATGGGAA
ASNS	TGTTGGATGGTGTGTTTGCATTT	GTCGCGGAGTGCTTCAATGT
PHGDH	GAACACCCCCAATGGGAACA	GCCTGGGGAATCTGCCTG
β-ACTIN	CTCCATCCTGGCCTCGCTGT	GCTGTCACCTTCACCGTTCC

Supplementary Table 2: Relationships between SLC1A5 expression and the clinicopathological characteristics of NSCLC patients.

Variables	SLC1A5 staining			Total	*P value*
	High (%)	Middle (%)	Low (%)		
Gender					
Female	30 (33.7)	51 (57.3)	8 (8.9)	89	0.7565
Male	39 (30.0)	81 (62.3)	10 (7.7)	130	
Age					
≤50	19 (32.8)	31 (53.4)	8 (13.8)	58	0.1627
>50	50 (31.1)	101 (62.7)	10 (6.2)	161	
Pathologic type					
LUAD	34 (25.6)	85 (63.9)	14 (10.5)	133	0.0345
LUSC	35 (40.7)	47 (54.6)	4 (4.7)	86	
Lymph node metastasis					
Negative	38 (27.5)	83 (60.1)	17 (12.3)	138	0.0087
Positive	31 (38.3)	49 (60.5)	1 (1.2)	81	
Distant metastasis					
M0	64 (31.1)	124 (60.2)	18 (8.7)	206	0.5087
M1	5 (38.5)	8 (61.5)	0 (0.0)	13	
Tumor stage					
I~II	19 (21.6)	55 (62.5)	14 (15.9)	88	0.0005
III~IV	50 (38.2)	77 (58.8)	4 (3.1)	131	
EGFR status					
Negative	15 (36.5)	24 (58.5)	2 (4.9)	41	0.6303
Positive	7 (25.9)	18 (66.7)	2 (7.4)	27	

Supplementary Table 3: The relationship between the level of SLC1A5 and tumor stage and lymphatic metastasis in patients with LUAD and LUSC.

Variables	LUAD			*P value*	LUSC			*P value*
	High (%)	Middle (%)	Low (%)		High (%)	Middle (%)	Low (%)	
Lymph node metastasis								
Negative	21 (25.3)	48 (57.8)	14 (16.9)	0.0078	17 (30.9)	35 (63.6)	3 (5.5)	0.0434
Positive	13 (26.0)	37 (74.0)	0 (0.0)		18 (58.1)	12 (38.7)	1 (3.2)	
Tumor stage								
I~II	11 (22.4)	26 (53.1)	12 (24.5)	0.0003	8 (20.5)	29 (74.4)	2 (5.1)	0.0026
III~IV	23 (27.4)	59 (70.2)	2 (2.4)		27 (57.4)	18 (38.3)	2 (4.3)	

Supplementary Table 4: Anti-body and reagents used in this study

REAGENT or RESOURCE	SOURCE	IDENTIFIER
Antibodies		
Rabbit Polyclonal anti-SLC1A4	Proteintech	Cat#13067-2-AP
Rabbit Polyclonal anti-SLC1A5	Proteintech	Cat#20350-1-AP
Rabbit polyclonal anti-HK2	Proteintech	Cat#22029-1-AP
Rabbit polyclonal anti-PFKFB3	Proteintech	Cat#13763-1-AP
Rabbit polyclonal anti-MCT1	Proteintech	Cat#20139-1-AP
Rabbit polyclonal anti-GPI	Proteintech	Cat#15171-1-AP
Rabbit polyclonal anti-HIF1a	Proteintech	Cat#20960-1-AP
Rabbit polyclonal anti-GAPDH	Proteintech	Cat#10494-1-AP
Rabbit Polyclonal anti-C-MYC	Proteintech	Cat#10828-1-AP
Rabbit Polyclonal anti-BACH1	Proteintech	Cat#14018-1-AP
Rabbit Polyclonal anti-Alpha Tubulin	Proteintech	Cat#14018-1-AP
Rabbit Polyclonal anti-TBX4	ABclonal	Cat#A10691
Rabbit Polyclonal anti-TBX15	ABclonal	Cat#A10481
Chemicals, Peptides, and Recombinant Protein		
Seahorse XF 1.0 M glucose solution	Aligent	Cat#103577-100
Seahorse XF 100 mM pyruvate solution	Aligent	Cat#103578-100
Seahorse XF 200 mM glutamine solution	Aligent	Cat#103579-100
JQ1	MedChemExpress	Cat#HY-13030
Critical Commercial Assays		
Cell-Light EdU Apollo567 In Vitro Kit	Ribobio	Cat#C10310-1
Meilun Reactive Oxygen Species Assay Kit	Meilunbio	Cat#MA0219-1
Image-iT Hypoxia Reagents	Invitrogen	Cat#I14834
Annexin V-FITC Apoptosis Detection Kit	KeyGEN BioTECH	Cat#KGA108
Human Gln ELISA Kit	RENJIEBIO	Cat#RJ12495
Human GSH ELISA Kit	RENJIEBIO	Cat#RJ12496
Seahorse XF Cell Mito Stress Test Kit	Aligent	Cat#103015-100
Seahorse XF Glycolysis Stress Test Kit	Aligent	Cat#103020-100
UltraSYBR One Step RT-qPCR Kit	CWBIO	Cat#CW0659
HiScript Q RT SuperMix for qPCR	Vazyme	Cat#R123-01
ChIP Assay Kit	Beyotime	Cat#P2078

Supplemental Figures

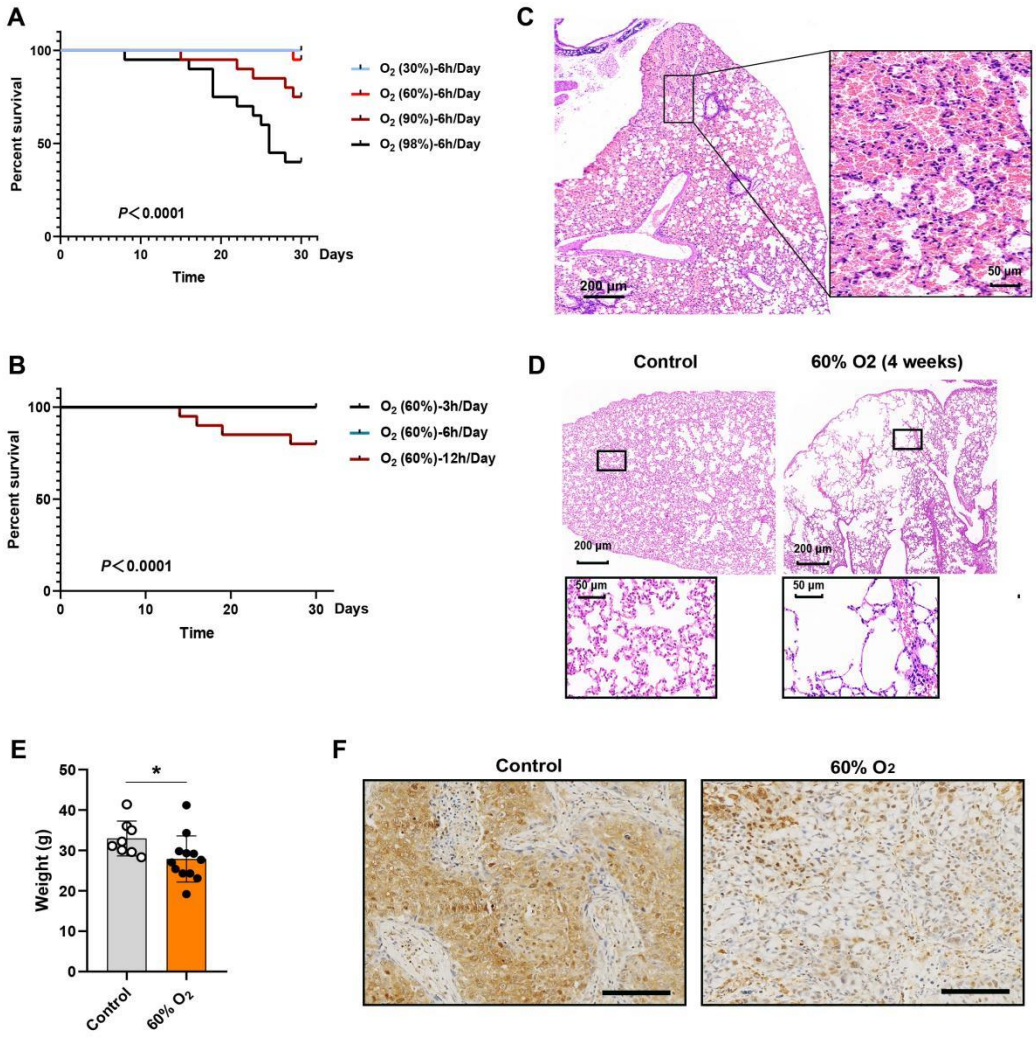

Figure S1. The anti-tumor activity and side effects of IH treatment.

(A, B) Oxygen concentration exceeding 90% or breathing of 60% oxygen for 12 h/Day result in death of tumor-free mice, log-rank test.

(C) Representative H&E staining of lungs with 98% O_2 treatment, bar (left)=200 μm, bar (right)=50 μm.

(D) Representative H&E staining of lungs with 60% O_2 (12 h/Day) treatment, bar (up)=200 μm, bar (down)= 50 μm.

(E) Quantitative analysis of body weight of mice treated with IH treatment (n=12) and the controls (n=8), two-tailed Student's t-test.

(F) Representative images of HMGA2-stained lung sections, bar=100 μm.

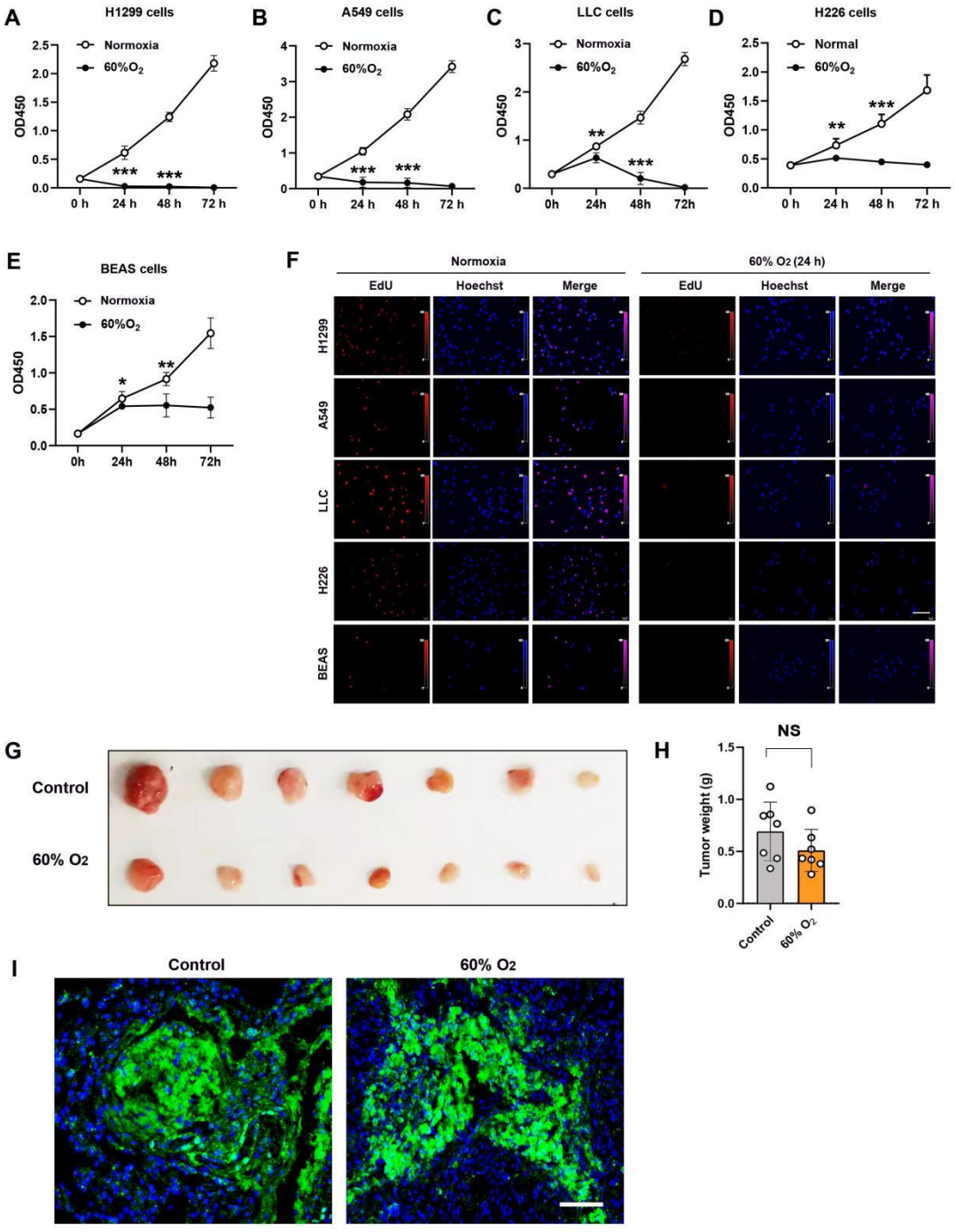

Figure S2. The effect of hyperoxia treatment on the proliferation of BEAS-2b cells and lung cancer cell lines.

(A-E) CCK-8 assay analysis of cell proliferation in H1299, A549, LLC, H226 and BEAS-2b cells (n=5). *$P<0.05$, **$P<0.01$, ***$P<0.001$ vs the normoxia group, two-tailed Student's t-test.

(F) Representative images of EdU and hoechst staining in H1299, A549, LLC, H226 and BEAS-2b cells with 60%O_2 (24 h) treatment, bar=50 μm.

(G, H) IH treatment has no significant effect on the growth of xenograft tumors (n=7), NS, $P > 0.05$ vs the control group, two-tailed Student's t-test.

(I) Image-iT green hypoxia reagent is used to detect hypoxia area in xenograft tumors, bar=100 μm.

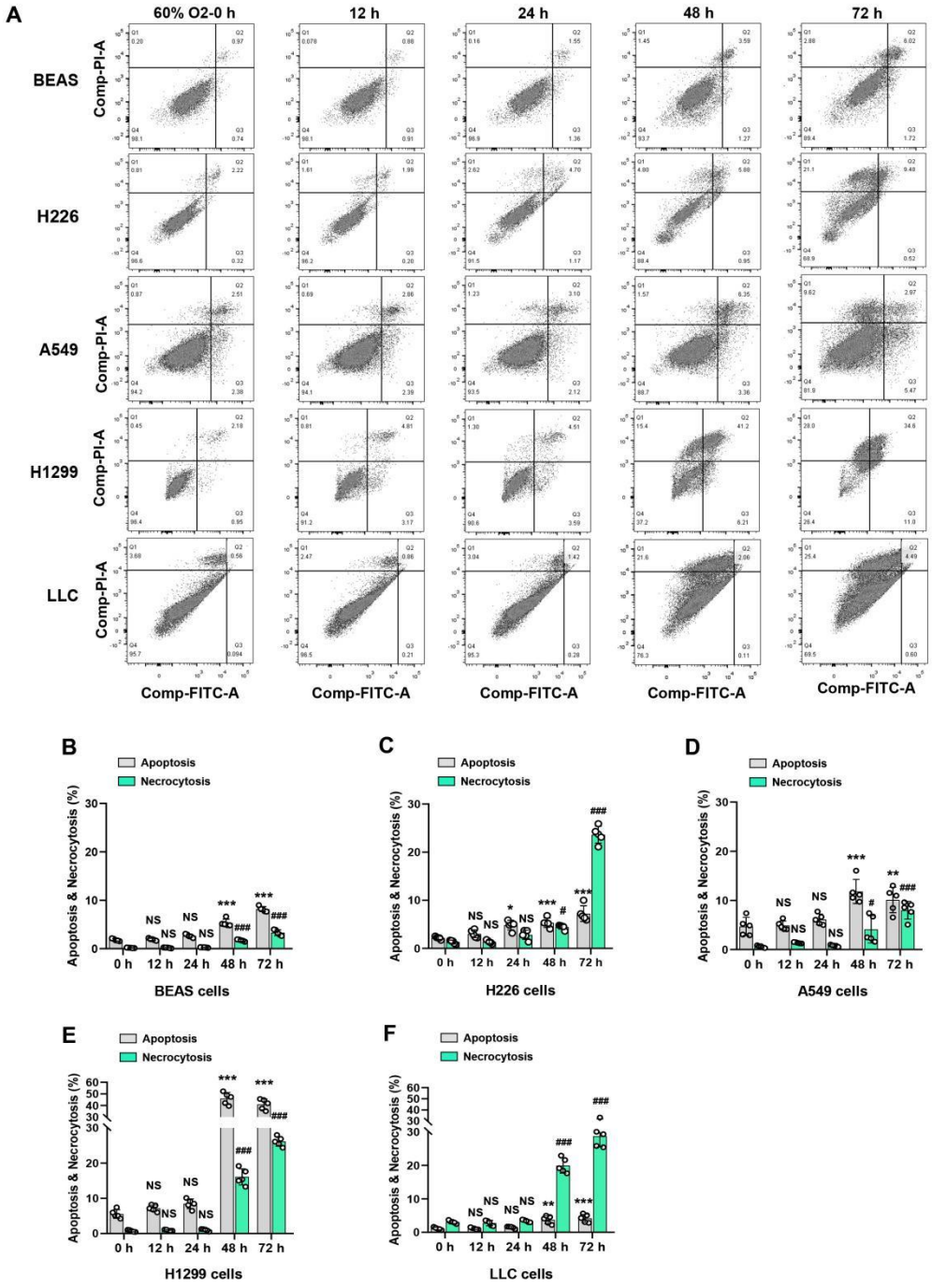

Figure S3. The effects of hyperoxia on cell apoptosis and necrocytosis.

(A-F) Flow cytometric analysis of cells apoptosis and necrocytosis in BEAS-2b, H1299, A549, H226 and LLC cells (n=5). $^{*}P<0.05$, $^{**}P<0.01$, $^{***}P<0.001$, $^{\#}P<0.05$, $^{\#\#\#}P<0.001$, NS, $P>0.05$ vs the 60% O_2 (0 h) group, respectively, one-way ANOVA followed by the Tukey's post hoc test.

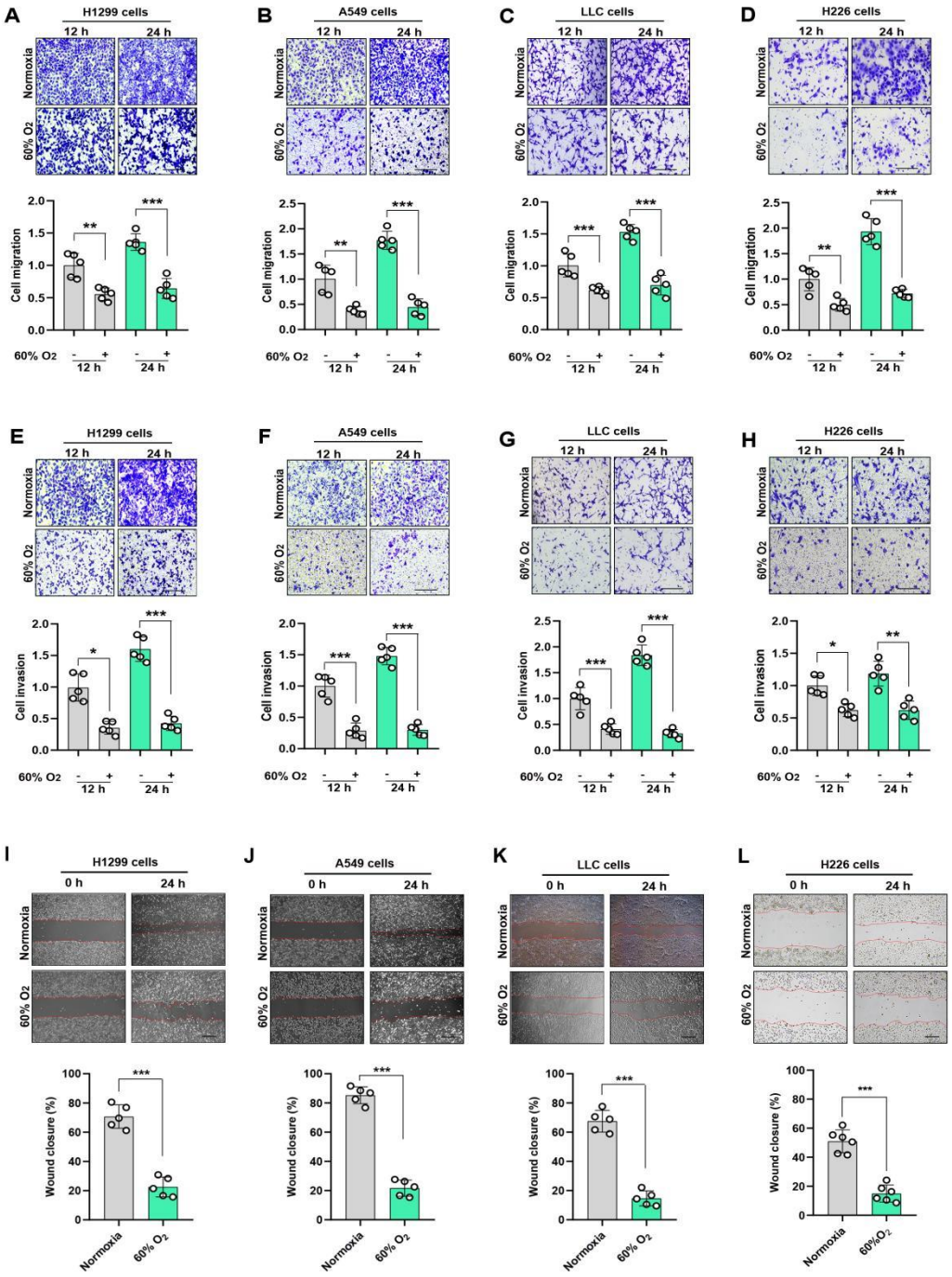

Figure S4. The effects of hyperoxia on cell migration and invasion.

(A-D) Hyperoxia treatment (60% O_2) suppress cell migration in H1299, A549, H226 and LLC cells, bar=50 μm.

(E-H) Hyperoxia treatment (60% O_2) suppress cell invasion in H1299, A549, H226 and LLC cells, bar=50 μm.

(I-L) The wound healing assay was further performed to determine the effect of 60% O_2

(24 h) on the migration of H1299, A549, H226 and LLC cells (n=5), bar=100 μm.

*P＜0.05, **P＜0.01, ***P＜0.001 vs the indicated group, two-tailed Student's t-test.

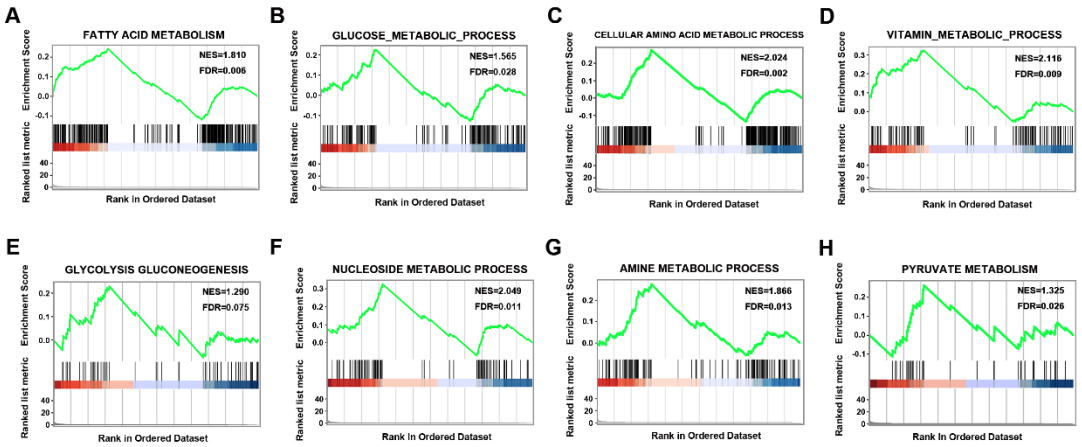

Figure S5. GSEA analysis show significant changes in metabolic pathways in hyperoxia treated H1299 cells.

(A-H) Gene set enrichment analysis of significant differentially expressed mRNA with normalized enrichment score (NES) and false-discovery rate (FDR) Q value.

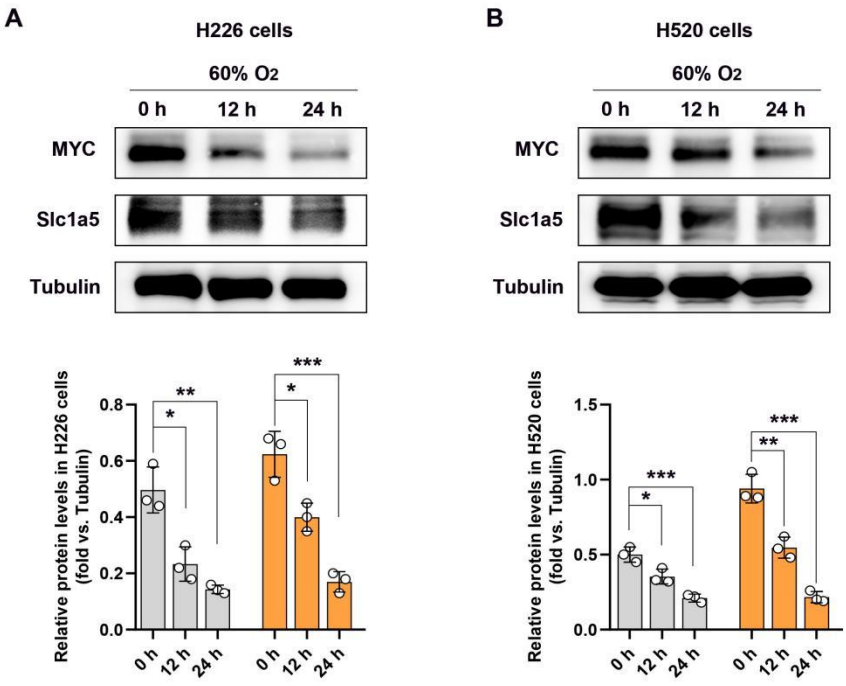

Figure S6. The effects of hyperoxia on the expression levels of MYC and SLC1A5 in LUSC cell lines.

(A) Western blot analysis for the expressions of SLC1A5 and MYC in H226 cells (n=3).

(B) Western blot analysis for the expressions of SLC1A5 and MYC in H520 cells (n=3).

*$P<0.05$, **$P<0.01$, ***$P<0.001$ vs the indicated group, one-way ANOVA followed by the Tukey's post hoc test.

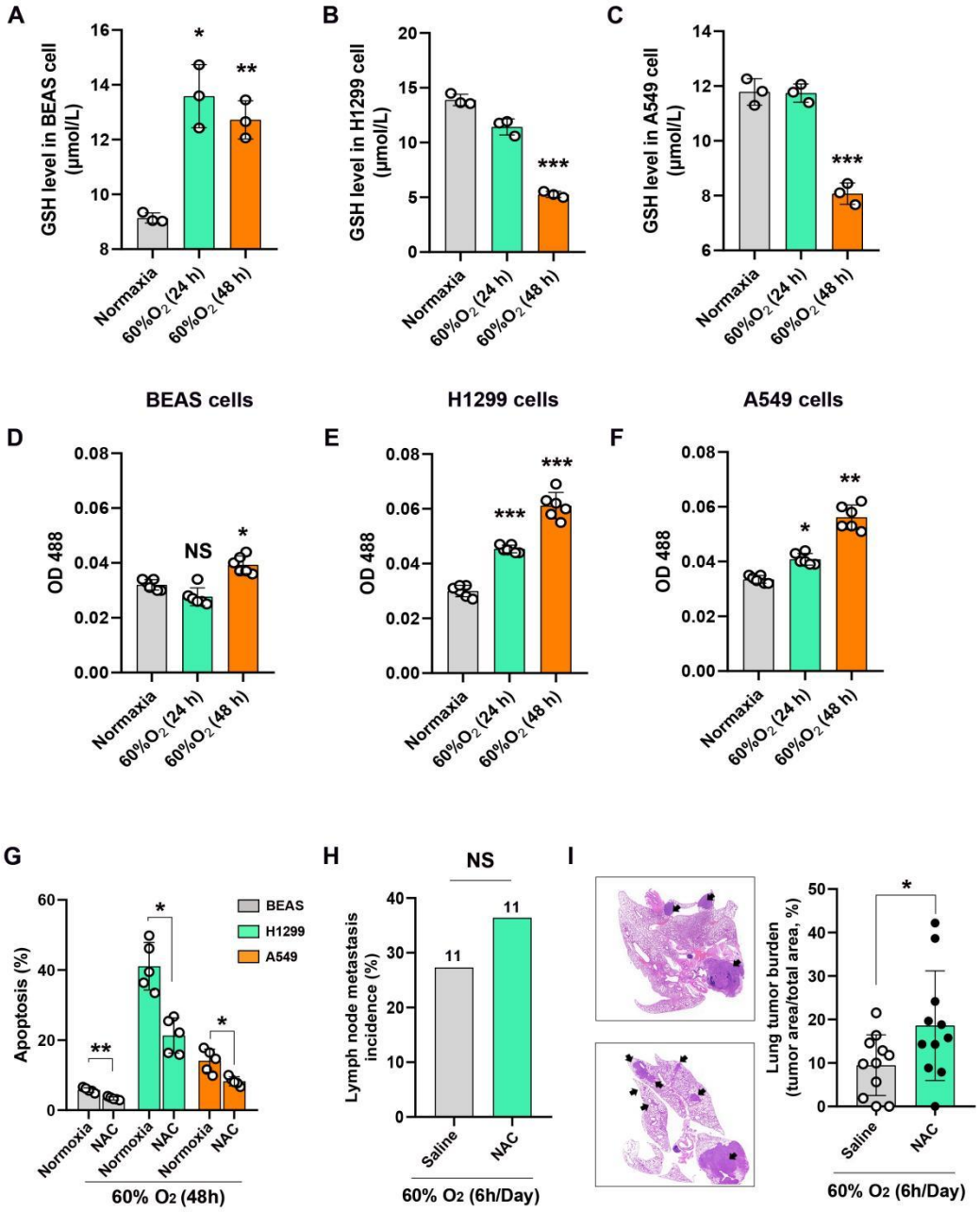

Figure S7. Hyperoxia treatment affects the cellular redox homeostasis of lung cancer cells.

(A-C) Effect of hyperoxia treatment on the levels of glutathione in BEAS-2b, H1299 and A549 cells (n=3).

(D-F) Effect of hyperoxia treatment on the levels of ROS in BEAS-2b, H1299 and A549 cells (n=5).

(G) Flow cytometric analysis of cell apoptosis in BEAS-2b, H1299 and A549 cells incubated with 2 nM NAC (n=5).

(H) Percentage of mice with lymph node metastases ($P>0.05$). NAC is administered in drinking water (1g/L) until the lungs are harvested (n=11), Chi-square test.

(I) Lung tumor burden in mice four weeks after *i.v.* injection of H1299 cells and representative lung section.

*$P<0.05$, **$P<0.01$, ***$P<0.001$, NS, $P>0.05$ vs the normoxia or indicated group, two-tailed Student's t-test.

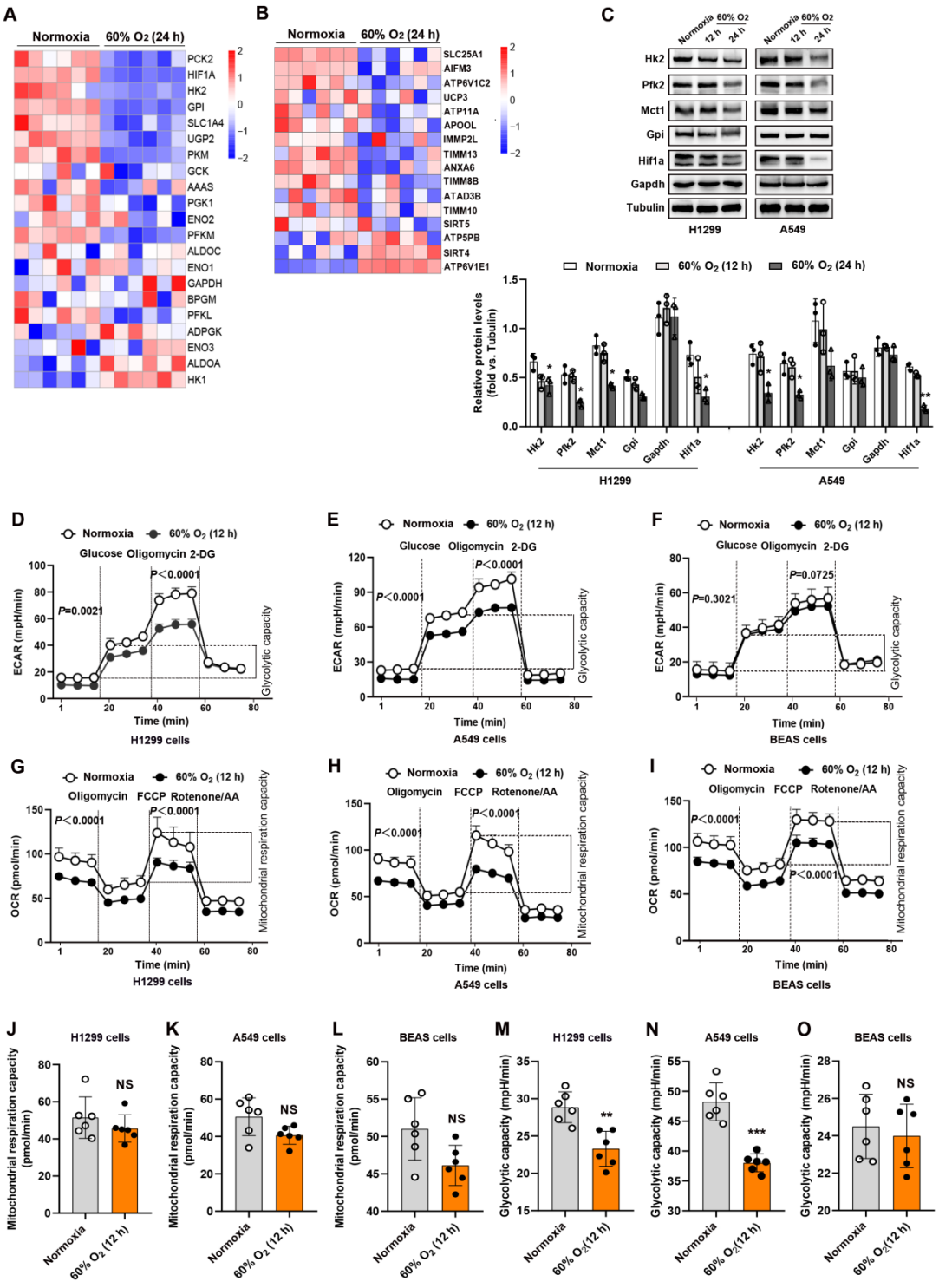

Figure S8. Hyperoxia treatment inhibits glycolysis in lung cancer cell lines.

(A) Heat map depicting changes in the expression of genes involved in “glycolysis” in H1299 cells.

(B) Heat map depicting changes in the expression of genes involved in “mitochondrial

inner membrane” in H1299 cells.

(C) Relative protein expression levels of PFK2, HK2, MCT1, GPI, HIF1α and GAPDH in H1299 and A549 cells treated with 60% O_2 (n=3).

(D-I) Measurements of ECAR and OCR in H1299, A549 and BEAS-2b cells treated with 60% O_2.

(J-O) Effects of hyperoxia treatment on the mitochondrial respiration capacity and glycolytic capacity in H1299, A549 and BEAS-2b cells (n=5).

*$P < 0.05$, **$P < 0.01$, ***$P < 0.001$, NS, $P > 0.05$ vs the normoxia group, two-tailed Student’s t-test.

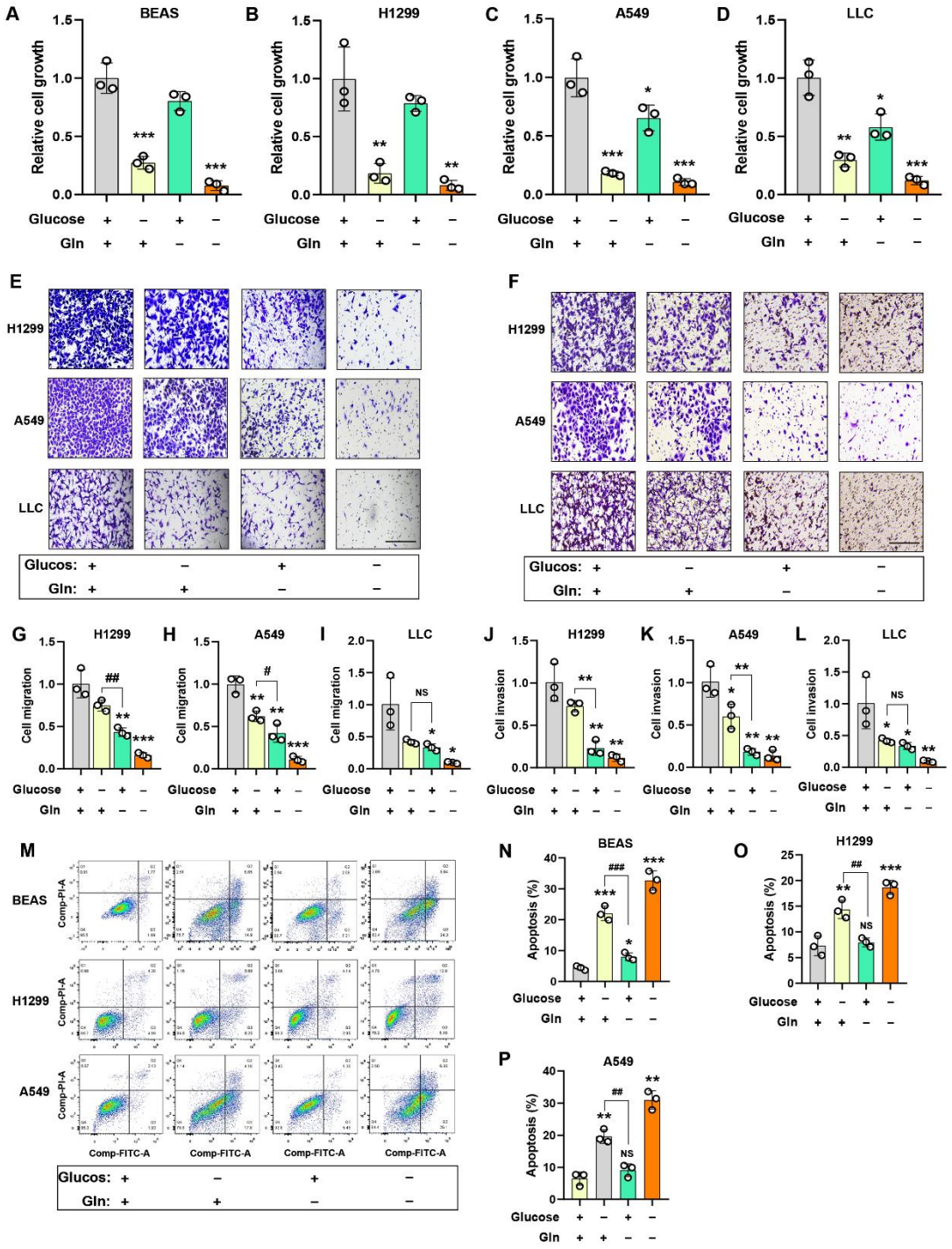

Figure S9. The progression of lung cancer depends on glucose and glutamine catabolism.

(A-D) Effects of glucose deprivation and glutamine deprivation on the proliferation of BEAS-2b, H1299, A549 and LLC cells (n=3). Cells were plated in complete media which was replaced the following day with glucose-free or glutamine-free medium supplemented with 10% fetal bovine serum.

(E-L) Effects of glucose deprivation and glutamine deprivation on the migration and invasion of H1299, A549 and LLC cells (n=3), bar=50 μm.

(M-P) Flow cytometric analysis of cells apoptosis in BEAS-2b, H1299 and A549 cells (n=3).

*P＜0.05, **P＜0.01, ***P＜0.001 vs the control group; $^{\#}P$＜0.05, $^{\#\#}P$＜0.01, $^{\#\#\#}P$＜0.001, NS, P＞0.05 vs the indicated group, one-way ANOVA followed by the Tukey's post hoc test.

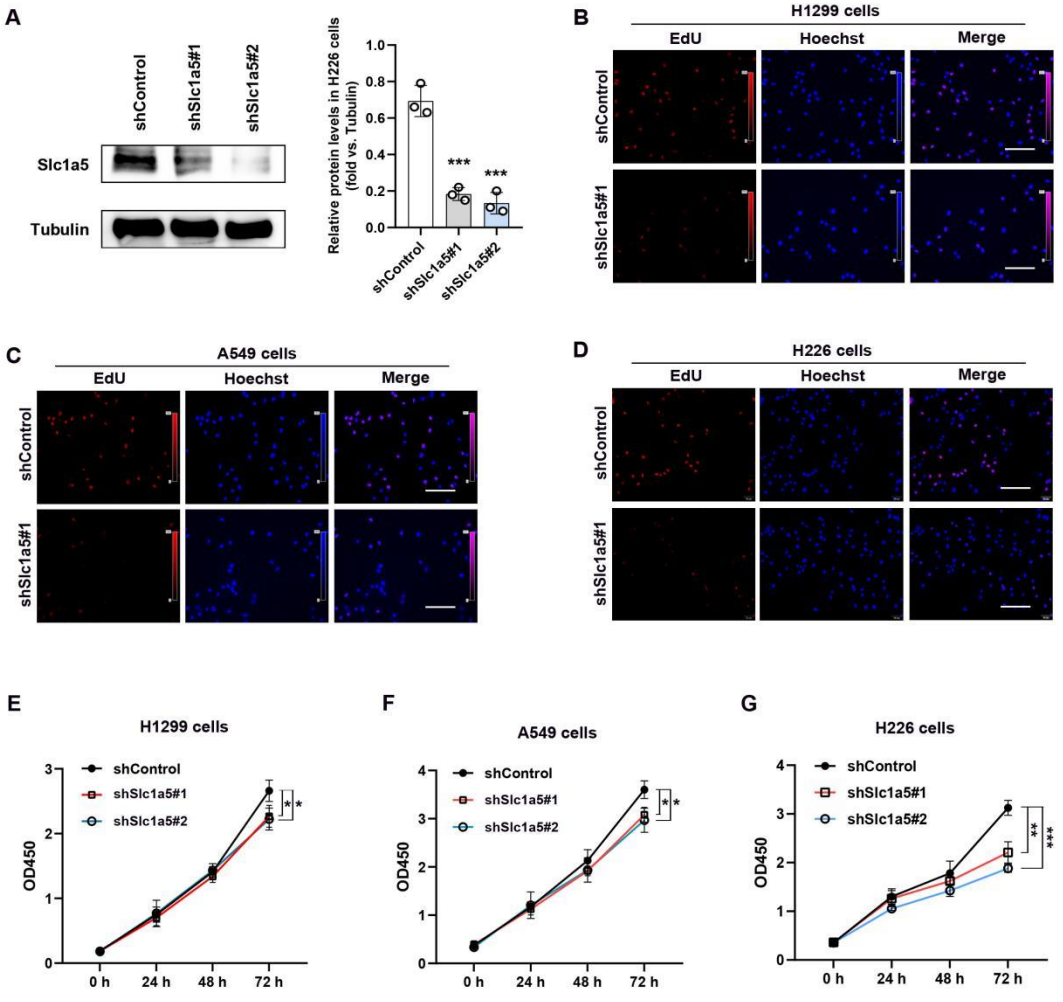

Figure S10. Knockdown of SLC1A5 inhibits the proliferation of H1299, A549 and H226 cells.

(A) Knockdown of SLC1A5 was confirmed at the protein level in H226 cells (n=3).

(B-D) Representative images of EdU and hoechst staining in H1299, A549 and H226 cells,

bar=50 μm.

(E-G) CCK-8 assay analysis of cell proliferation in H1299, A549 and H226 cells (n=5). *P ＜0.05, **P＜0.01, ***P＜0.001 vs the shControl group, two-tailed Student's t-test.

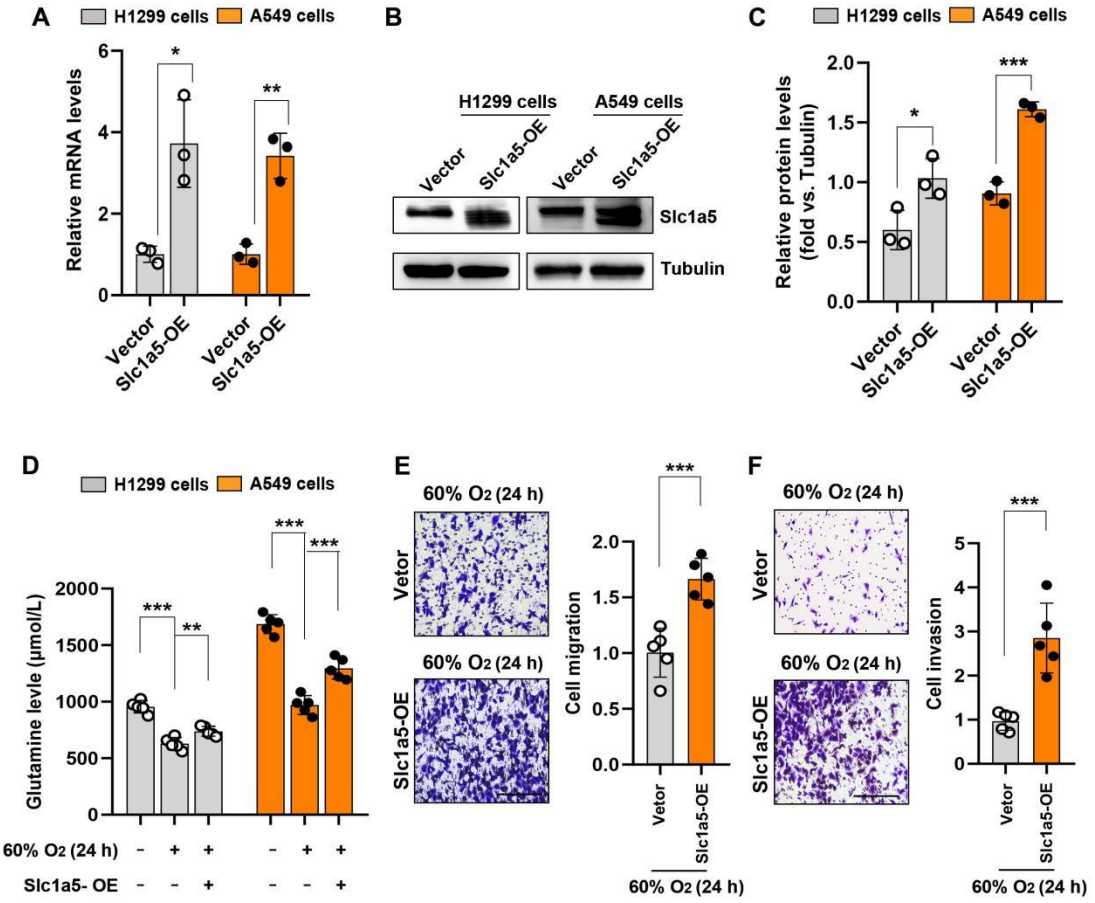

Figure S11. SLC1A5 overexpression increase the intracellular glutamine and cell invasiveness in lung cancer cells with hyperoxia treatment.

(A-C) The gene transfection efficiency was detected by PCR and Western blot analysis in H1299 and A549 cells (n=3).

(D) The levels of glutamine in H1299 and A549 cells (n=5).

(E, F) Effect of SLC1A5 overexpression on the migration and invasion of 60% O_2 (24 h) treated H1299 cells, bar=50 μm.

*P＜0.05, **P＜0.01, ***P＜0.001 vs the indicated group, two-tailed Student's t-test.

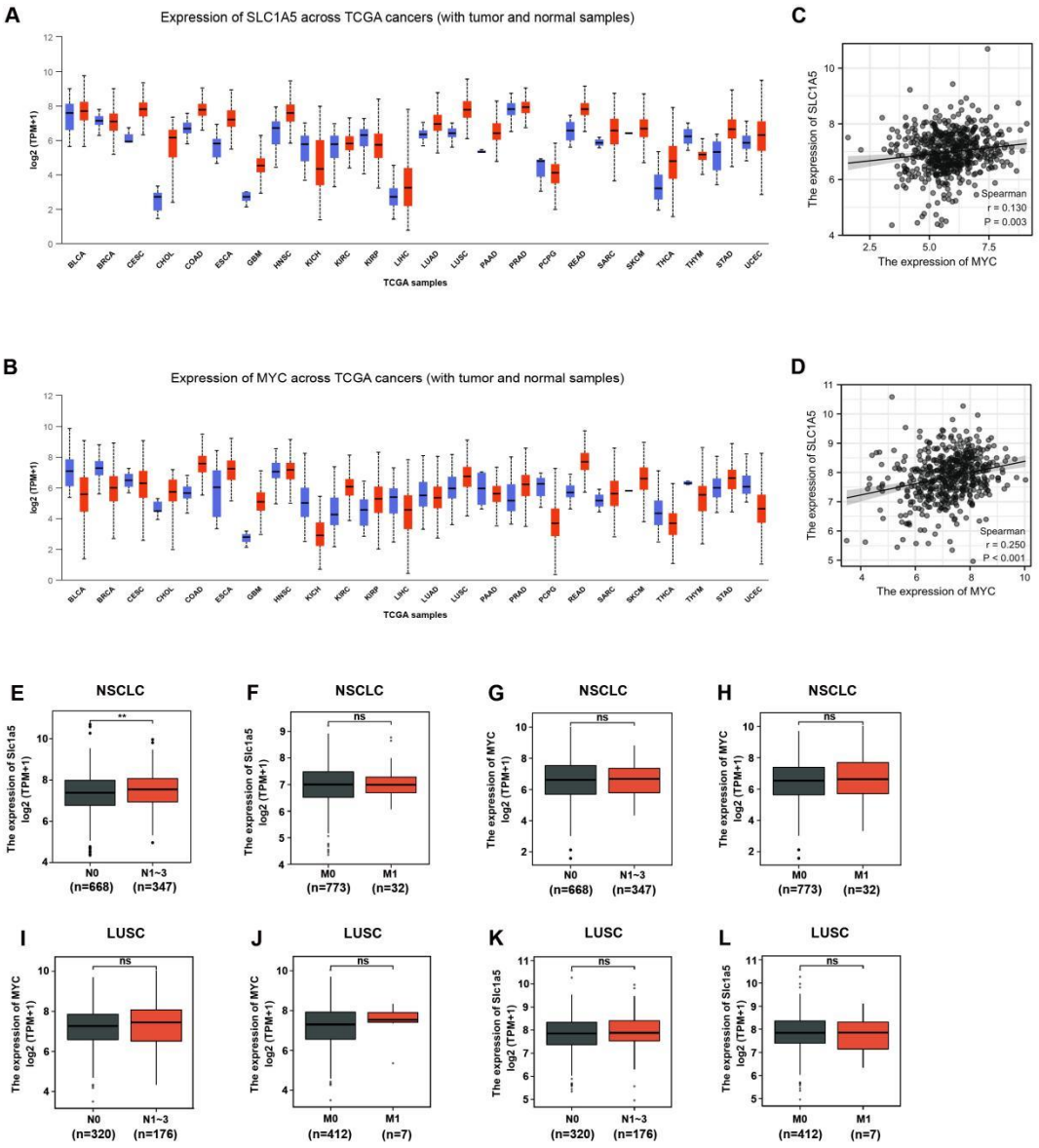

Figure S12. The expression levels of SLC1A5 and MYC are closely related to the clinical characteristics of patients with NSCLC.

(A, B) The expressions of MYC and SLC1A5 in NSCLC tissues and normal tissues was analyzed according to TCGA database.

(C) Correlation between mRNA levels of SLC1A5 versus MYC in LUAD tissues according to TCGA database, r=0.130, *P*=0.003.

(D) Correlation between mRNA levels of SLC1A5 versus MYC in LUSC tissues according to TCGA database, r=0.250, $P<0.001$.

(E, F) Slc1a5 is increased in NSCLC patients with lymph node metastasis.

(G, H) There was no significant difference in MYC expressions between NSCLC patients with or without metastasis.

(I-L) There was no significant difference in MYC and SLC1A5 expressions between LUSC patients with or without metastasis.

**$P<0.01$, NS, $P>0.05$ vs the N0 or M0 group, two-tailed Student's t-test.